ENHANCED ELECTRICAL TRANSPORT IN LiBr-AL$_2$O$_3$ MULTIPHASE MIXTURE

A Thesis Submitted
In Partial Fulfilment of the Requirements
for the Degree of
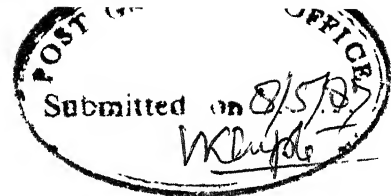## MASTER OF TECHNOLOGY

by
SHIULI GUPTA

to the

MATERIALS SCIENCE PROGRAMME

INDIAN INSTITUTE OF TECHNOLOGY, KANPUR

MAY, 1987

MSP· 1987—M— GUP.. ENH

Certificate

Certified that this work on " Enhanced Electrical Transport in LiBr-Al$_2$O$_3$ Multiphase Mixture " by Shiuli Gupta has been carried under my supervision and that this has not been submitted elsewhere for a degree.

(K. Shahi)

Assistant Professor
Materials Science Programme
Indian Institute of Technology,
KANPUR

ACKNOWLEDGEMENTS

CONTENTS

--

LIST OF FIGURES

LIST OF TABLES

--

ABSTRACT

With a view to develop new dispersed solid electrolyte systems (DSES) for high energy density batteries and other electro-chemical devices, mixtures of varying composition of γ-Al_2O_3 in LiBr were studied. The complex impedance analysis together with conventional a.c. (1 khz) conductivity measurements has been extensively used to study the electrical transport properties of the DSES. Detailed study of conductivity as a function of frequency, temperature, composition and particle size of the dispersoids have been carried out.

The maximum enhancement in conductivity was observed for LiBr containing 10 m/o γ-Al_2O_3 of 0.05 μm size. The enhancement was at least 4 orders of magnitude at 84°C. Although the exact mechanism of enhancement could not be specified, the Jow and Wagner space charge layer model was found satisfactory. SEM studies were not very instructive due to the hygroscopic nature of the samples.

CHAPTER - 1

INTRODUCTION

Electrochemical systems are needed for the reversible storage of electrical energy to be used in utility load levelling, electric vehicle propulsion, solar electric storage, electronic devices etc. Fast ion transport in solids plays a critical role in a number of energy storage and production systems, such as batteries, fuel cells, magnetohydrodynamics, hydrogen storage oxidation catalysts etc. Batteries comprise three active components, the anode or electropositive electrode, the cathode or electro-negative electrode and the electrolyte that separates them but permits the transfer of ionic species between them without allowing any electronic transport. While the composition of the electrodes (anode and cathode) must change during reaction i.e. when the cell is charged or discharged, that of the electrolyte should not. Furthermore, while the cell parameters such as open circuit voltage (OCV), energy density etc. are determined by the electro-chemical properties of the anodes and, cathodes the current rate capabilities are determined by the conduction properties of the electrolyte. Apparently there are a number of choices as far as anodes and cathodes are concerned, but it is not so for the electro-lytes. At present therefore considerable effort is being made to develop new and better solid electrolytes.

1.1 SUPERIONIC CONDUCTORS:

Superionic conductors or fast ionic conductors or solid electrolytes exhibit ionic conductivities that can be as large as $1 \ \Omega^{-1} cm^{-1}$ at temperatures ranging from a little above room

temperature to ceramic temperatures of the order of 1800°K. They are different from the conventional ionic conductors mainly due to the vast difference in the magnitude of ionic conduction. For example, taking an extreme case, the ionic conductvity of the superionic conductor $RbAg_4I_5$ is several orders of magnitude greater than that of NaCl at the same temperature.

According to Rice and Roth (1971) these highly conducting solids can be broadly divided into three main groups. These are given below.

1.1.1 Cationically Disordered Fast Ion Conductors:

This includes, the ionic compounds of the type typified by the cation disordered phases of the silver, copper, and Lithium halides, chalcogenides, sulphates etc. The ionic compounds belonging to this group can be structurally characterized as having a relatively rigid crystalline frame work composed of the non-conducting ionic species (usually the anion) with the conducting cation species distributed in a statistically disordered fashion among the available sites offered by the rigid non-conducting framework. There are usually several, and sometimes many, possible sites per conducting species. The exceptionally high ionic conductivities of these solids result from the almost liquid-like state of the disordered cation species. Some examples are,

α -AgI α -Li_3N

α -Ag_2S α -Ag_2Se

α -Ag_2Te α -Ag_3SBr

$$RbAg_4I_5 \qquad\qquad K\,Ag_4I_5$$

$$RbCu_4(Cl_3I_2) \qquad\qquad \alpha - Li_2SO_4$$
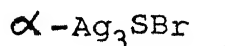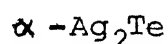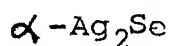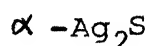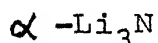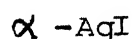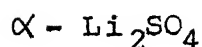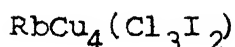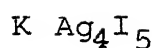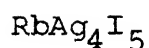
1.1.2 β-Aluminas:

The isomorphous series of hexagonal compounds exhibiting the so called beta-alumina structure

$$A_2O.\ n\ N_2O_3 \qquad \begin{array}{l} (A = Na,K,Rb,Ag,Li,Tl \\ (\\ (M = Al,Ga,Fe^{3+} \\ (\\ (n = 5\text{--}11\ (integer) \end{array}$$
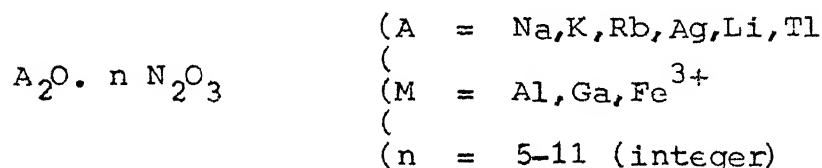
In the beta-alumina group of ionic compounds cation conduction (A^+) takes place in planes which separate the non-conducting crystalline spinel-blocks of the beta-alumina structure. The conducting plane is characterized by a two-dimensional hexagonal array of O^{2-} anions, with the (A^+) ions distributed in a random fashion over the two dimensional manifold of possible cation sites defined by the fixed anion network. Thus, the essence of cation disorder that is responsible for the high ionic conductivity of these solids may be regarded as a two-dimensional counterpart of that found in the first group of ionic solids.

1.1.3 Stabilized Zirconia Type:

The defect stabilized ceramic oxides of the calcium fluoride structure, e.g.,

$$CaO.AO_2 \quad (A = Zr,\ Hf,\ Th,\ Ce)$$

$$M_2O_3.ZrO_2 \quad (M = La,Sm,Y,Y6,Sc\ )$$
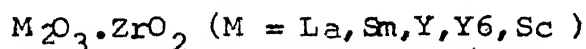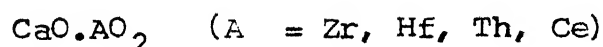
In this group of ionic conductors, anion (O^{2-}) transport is animated

by a relatively large and fixed number of (O^{2-}) vacancies produced by the stabilizing agen on account of the requirement of overall change neutrality. For example in the case of $CaO.ZrO_2$, known in literature as calcia stabilized zirconia (CSZ), we may write the explicit chemical formula $Ca_x^{2+} \ Zr_{1-x}^{4+} \ O_{2-x}^{2-}$ where x denotes the fractional concentration of Ca. Thus, in this example, the addition of the stabilizing agent Ca introduces a fixed concentration of x/2 vacancies in the anion (O^{2-}) component. The study of ionic conductivity in this group of compounds has been particularly interesting

Ionic conductivity of these oxides becomes high at elevated temperatures and hence these materials are suited for high temperature applications such as fuel cells etc.

1.2 Li BASED SOLID ELECTROLYTES :

Li-based electrochemical cells are of considerable interest because of the following reasons:

  i. Low equivalent weight of Li metal

 ii. High electropositivity of Li which gives rise to high cell
      voltages and energy densities.

iii. Li metal is not expensive and technically easy to handle,
      if certain restrictions are considered.

Thus it is of specil interest to find suitable solid Li-electrolytes which can be used in Li based cells.

The three main requirements for solid Li-electrolytes are high Li-ion conductivity of at least $1 \times 10^{-3} \ \Omega^{-1} cm^{-1}$ at the operating temperature of the cell, confined with a negligible

partial electronic conductvity, stability of the electrolyte
in contact with the electrodes of high Li activities and the
production of a suitable polycrystalline sinter which is cheap
and easy to fabricate.

The Li-electrolytes can be divided into several groups
based on their crystal structures. This allows us to discuss the
disorder mechanism which is responsible for the Li-ion diffusion
in the respective structures.

1.2.1 Solid Li-Conductors with The Rocksalt Structure:

Lithum halides (LiX, X = F,Cl,Br,I) especially LiI
are well known as solid Li-electrolytes. (Jackson, 1969]. These
compounds crystallize in the rocksalt structure, with Li ions in
octahedral sites. (Fig. 1.1). The large ionic radius of the
iodine ion creates a lattice which gives the small Li ions enough
space for thermally activated diffusion. There is no structurally
preferred direction for diffusion, so that the ionic conductivity
is expected to be isotropic. All Li-halides including LiI
exhibit Schottky type of defect in which equal number of cation
and anion vacancies exist. The cation vacancies are more mobile
than the anion vacancies. Since the concentration of those point
defects increases rapidly with temperature, the ionic conductivity
also shows a strong temperature dependence.For the determination
of d.c. ionic conductivity, a.c. impedance of the electrochemical
cells in certain frequency range usually 1MHz $>$ f $>$ 10Hz is
measured. The complex plane impedance diagram of LiI with
reversible Li-electrodes is shown in Fig. 1.1 b as reported by
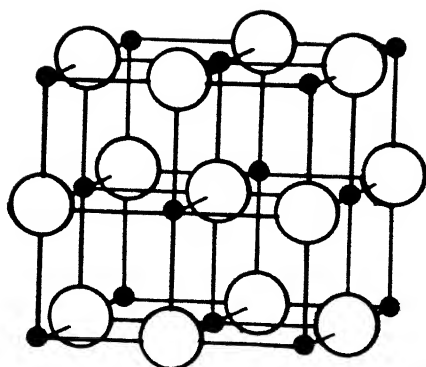
(a) Rocksalt structure
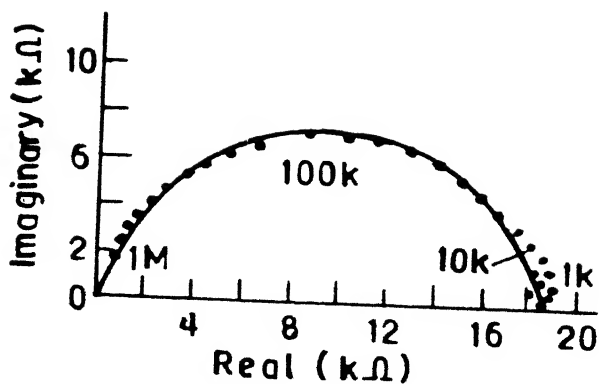
(b) Impedance spectrum
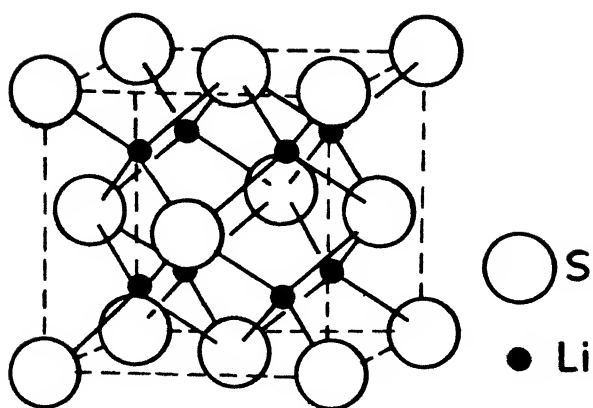
(c) Antifluorite structure
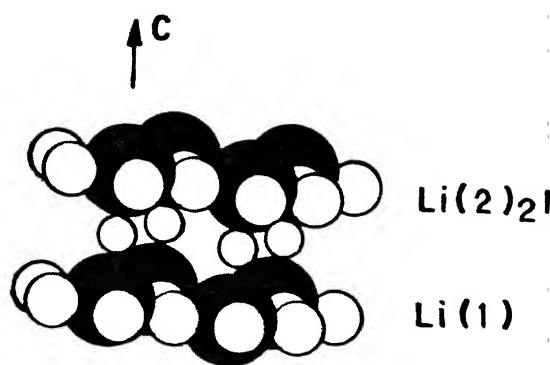
(d) Li_3N Structure

FIG. 1·1

Alpen et·al (1978). The semicircle in impedance diagram is due to a parallel combination of the bulk electrolyte resistance Γ with the geometrical capacity of the cell Cg. The frequency at the maximum of the semicircle is given by,

$$f_{max} = \frac{\omega_{max}}{2\pi} = \frac{1}{2\pi R_E C}$$

An important step forward to a technological application has been the study of ionic conductivity in the two phase system LiI-Al$_2$O$_3$ by Liang (1973-1978). He claimed that it is possible to enhance the ionic conductivity in LiI by increasing γ-Al$_2$O$_3$ content. The ionic conductivity was found to be enhanced by three orders of magnitude in the LiI-Al$_2$O$_3$ system. As LiI has a room temperature conductivity of $10^{-7} \Omega^{-1} cm^{-1}$, this material i suitable only for low drain batteries which have separators in the form of extremely thin films. The LiI based electrolytes are stable with Li-metal.

1.2.2 Solid Li-conductors with the Antifluorite Structures:

The ionic conductivity in materials with fluorite structure such as doped ZrO$_2$ and ThO$_2$ can be explained by an anion vacancy mechanism. In analogy to these oxygen conductors it seems to be interesting to produce cationic conductors with a large amount of cation vacancies in an autifluorite type structure. Lithium oxide Li$_2$O and lithiumsulfide Li$_2$S are well known Li-compounds with antifluorite structures, the unit cell for Li$_2$S is shown in Fig. 1.1 b. It is possible to vary the Li$_2$O structure substituting

with trivalent metal ions M^{3+} (M = Al, Ga, Fe and Te) to get
materials of the form $Li_{5-2}M^{3+}O_4$ which form a superstructure
to the Li_2O structure. A very important compound in this group
is $Li_{1.8}N_{0.4}Cl_{0.6}$.

Table 1.1

Conductivity σ and activation energy for Li^+ conduction in
materials with rock salt structure

	σ_{300K} $\Omega^{-1}cm^{-1}$	σ_{500K} $\Omega^{-1}cm^{-1}$	E_a (eV)
Li_5AlO_4	1×10^{-9}	3.5×10^{-6}	0.41
$Li_{1.8}N_{0.4}Cl_{0.6}$	1×10^{-6}	1.2×10^{-3}	0.29

1.2.3 Solid Lithium Conductors with Layer Structures:

The best solid Li-ion conductors in this structure
group are (Li-Na) -alumina and Li_3N exhibiting room temperature
conductivities comparable to that of Na-B- alumina. The crystal
structure of the β -alumina based electrolytes is well known,
there exist two principal forms, the hexagonal β -and the
rhombohedral β'' -phase. A high disorder of the sodium ions on
the basal plane combined with the rapid exchange of the Na^+ ions
between the occupied Beevers-Ross (BR) and mid-oxygen sites and

1.4.2 Classical Doping Theory :

^{I}t is conceivable that by the dissolution of insulating particles (e.g., Al_2O_3) in an ionic solid (e.g., CuCl), copper vacancies are created as follows.

$$Al_2O_3 = 2Al_{Cu}^{\cdot\cdot} + V'_{Cu} + 3O'_{Cl}$$

If this were the mechanism for the conductivity enhancement, one would expect that a few mole percent of alumina would be sufficient to reach a concentration of vacancies required to attain an increase of one to two orders of magnitude in the conductivity. Since the solubility of alumina in cuprous chloride was not detectable and the experimental results showed that about 20 m/o alumina with no dissolution was necessary to attain a two orders of magnitude increase in conductivity, the classical doping theory cannot be used to explain the conductivity enhancement in the dispersed phase solid electrolytes such as CuCl (Al_2O_3), AgI (Al_2O_3) etc.

1.4.3 Wagner's Model on Semiconductors Containing Inclusions of Another Phase:

Wagner (1957) applied the concept of electrical double layer at the interface of a two phase mixture to calculate the electrical conductivity of metal oxide, MO_x, involving inclusion of metal, M, particles as a second phase. He considered the cases where the electronic concentration, n , is everywhere much greater than the concentration of electrons and other charged defects in the metal oxides free of inclusions. The electron

and Li_3PO_4 had high conductivities. Li_4SiO_4 is characterized by a disordered cation lattice with 8 Li-ions distributed over 18 sites. The addition of Li_3PO_4 introduces intestitial Li sites which contribut to the conductivity. The closely related structures of Li_4SiO_4 and Li_3PO_4 can be described by isolated (SiO_4) or (PO_4) tetrahedra linked together by a large number of Li sites. This solid solution is characterized by a conductivity of $10^{-3} \Omega^{-1} cm^{-1}$ at 230°C.

A compound which has recently attracted the interest of electrochemists is the $Li_{14}Zn (GeO_4)_4$ (LISICON) found by N.Y.-P.Hong (1978). It should be noted that LISICON is not stable in contact with lithium, therefore, a technical. application seems to be questionable.

Table 1.2

Conductivity σ and activation energy E for Li-ion conduction in materials with layer structure

	σ_{300K} $\Omega^{-1} cm^{-1}$	$\sigma \sigma_{400K}$ $\Omega^{-1} cm^{-1}$	E_a (eV)
Li-Na β - alumina (Li/Na 8)	7.5 x 10^{-4}	2.1 x 10^{-3}	0.08
(Li-Na) β -alumina (Li/Na = 1.1)	5.10^{-3}	--	--
Li_3N	2.5 x 10^{-3}	2.14 x 10^{-2}	0.15

Table 1.3

Conductivity σ and activation energy E_a for Li-ion conduction in materials consisting of MO_4 (M = P, Si, Ge) tetrahedra.

	σ_{300K} $\Omega^{-1} cm^{-1}$	σ_{500K} $\Omega^{-1} cm^{-1}$	E_a (eV)
$LiAlSiO_4$	$-$	6.9×10^{-7}	0.47
$Li_{14}Zn(GeO_4)_4$	10^{-6}	4×10^{-3}	0.33
$Li_{3.6}Si_{0.6}P_{0.4}O_4$	6.2×10^{-7}	2.1×10^{-3}	0.34

1.3 THEORETICAL ASPECTS OF SOLID ELECTROLYTES:

In this section we discuss some theoretical efforts to explain two basic features of solid electrolytes: the origin of the formation of the substantial disordering required for the electrolytic conductivity in solid electrolytes and the transport mechanism in such disordered structures.

1.3.1 Sublattice Disorder:

In nearly perfect crystals, atomic (Ionic) diffusion is always connected to the existence of lattice defects. The most common types of diffusion in crystals are diffusion through vacancies and diffusion thro' interstitial sites. In ionic crystals, such motion of ions under the influence of an external field creates a net ionic current. The ionic conductivity σ is generally described by an Arrhenius Equation.

$$\sigma = (c/kT) \exp(-Ea/kT) \qquad \cdot \qquad (1.1)$$

where E_a is the activation energy of ion motion, c the pre-exponential factor, k the Boltzmann constant, and T the temperatur The constant c is given by,

$$c = (1/3)(Ze)^2 nd^2 \omega_o \qquad (1.2)$$

where Ze is the charge of the conduting ion, n is the density of defects, d is the jump distance of the ion, usually the closest ionic pair distance, and ω_o is the attempt frequency. The corresponding diffusion coefficient D is defined by

$$D = Do \exp(-Ea/kT) \qquad (1.3)$$

$$Do = c/(z^2 e^2 n) \qquad (1.4)$$

The diffusion coefficient D and ionic conductivity σ are related through well known Nerst-Einstein equation

$$\sigma = n (Ze)^2 D/(kT) \qquad (1.5)$$

It is clear from Eq. 1.2 that to have a large ionic conductivity in case of vacancy diffusion the number of vacancies must be large enough so that the effective number of ions contributing to the diffusion can be large. In other words, if one can find crystals in which the number of available sites is greater than the number of the diffusing ions so that the ions can distribute over these available sites at relatively low temperatures, one can expect a high ionic conductivity. For such solids to be rigid, the disorder

should occur only in one of the sublattices where diffusing ions exist.

Let us examine the situation with typically known solid electrolytes. One of the best known examples is -AgI. Here, the iodide ions form a rigid, body-centered cubic sublattice while the small Ag^+ ions (two per unit cell) distribute homogeneously in the twelve tetrahedral interstitial sites of the iodide lattice. Based on X-ray diffraction results with polycrystalline specimens Strock (1935) first pointed out that Ag^+ ions were distributed statistically over a large number of interstitial positions, and this situation was thought to be largely responsible for the high ionic conductivity of -AgI. This kind of situation where a small number of ions are forced to distribute over a large number of available sites has come to be called "sublattice disorder" ot " cation disorder" or "liquid sublattice"

In the more complex solid electrolytes, the conducting ions are distributed nonuniformly over crystallographically non-equivalent sites. However, the average activation energy of ionic motion is small relative to that of ordinary solids. In some fast ionic conductors, the activation energies are of the order of 0.1 to 0.2 eV. The smallness of the activation (and at the same time the the smallness of the pre-exponential factor) is indeed a better criterion for characterization of fast ionic conductors than the ionic conductivity itself. In some cases, the ionic conductivity changes very little, or even decreases, upon melting with similar activation energy and pre-exponential factor. Based on these

experimental evidences, it is at least evident that the "sublattice disorder" is responsible for the characteristics of fast ionic conduction.

Extremely low activation energies of some typical fast ionic conductors are, however, still hard to explain by structural features alone. It is an important theoretical test, to establish whether the magnitudes of the activation energies are solely determined by structural considerations or whether they depend mainly on the mechanism of ion transport and hence on the specific character of conducting ions. It has been shown that at least a part of the reduction in the magnitude of activation energy over that of the single ion motion can be attributed to cooperative motions of ions which occur in disordered systems.

1.3.2 Cooperative Ionic Motion:

In almost perfect crystals, the diffusion of ions takes place in the form of hopping. That is ions spend most of their time in their respective potential wells and the dwell time of ions in the potential wells is long compared to the hopping time of ions to neighbouring sites. The ions are located mostly in their specific lattice sites and the attempt frequency ω_o should be the ordinary vibrational frequency of crystal lattices or $10^{13} s^{-1}$. In fast ionic conductors conducting ions are distributed over a large number of available sites (sublattice disorder) and the activation energy of ionic motion is low. This indicates that the potential wells in which the conducting ions are located are shallow.

This situation also makes the attempt frequency low. At the same time, the amplitude of thermal motion becomes large as indicated by the results of diffraction experiments. Therefore, the motion of ions in these substances cannot, in general, be represented by a simple hopping diffusion.

The common description of ionic diffusion or conduction is based on one ion hopping in the lattice in terms of the random walk theory. It is, however very difficult to give reasonable explanations of extremely fast conduction with extremely low activation energies. within the framework of the random walk theory. To reconcile these difficulties, some models of cooperative motion of ions have been proposed.

One of the most commonly known cooperative motions of ions adopted in the theory of diffusion is the interstitialcy motion. Here, two ions, the one on an interstitial site and the other on an adjacent regular site, cooperate in such a way that the interstitial ion replaces the ion on the regular site while forcing the ion on the regular site out into an adjacent interstitial site. In this model, a row of ions move cooperatively by one atomic distance each through a vacancy so that, as a result, the vacancy moves a long distance nd, where n is the number of ions involved in the row and d is the atomic distance. It is apparent that such a cooperative motion, called the caterpillar mechanism, has a distinct advantage of increasing the jump distance if it occurs.

Cooperative motions of ions like those discussed above are found especially effective in disordered lattices in reducing
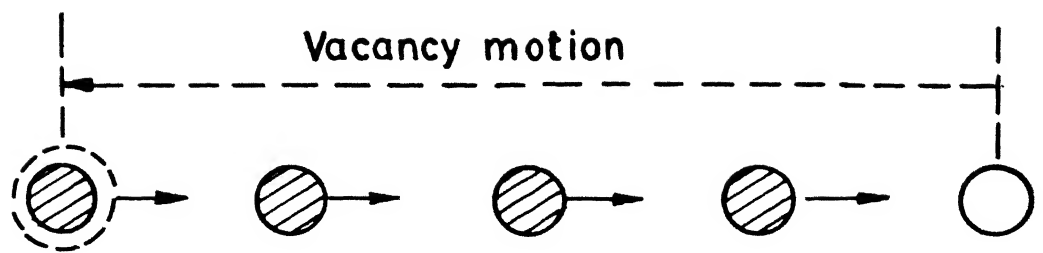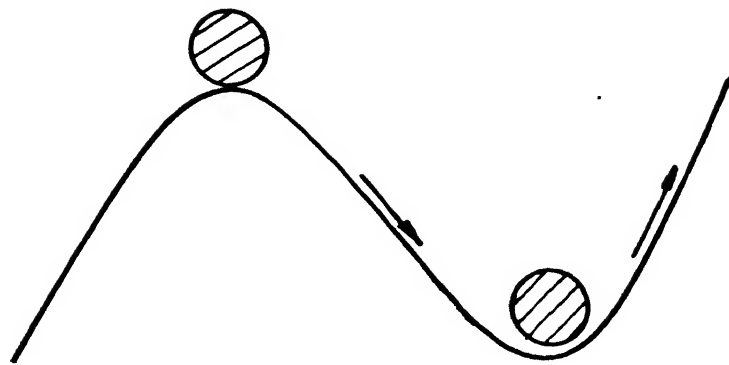
FIG. 1.2 (a) Caterpillar mechanism of ionic motion

(b) Cooperative motion of two ions with $E_a = 0$

the activation energy of motion of the groups of ions. In dis-
ordered lattices, due to the availability of extra interstitial
sites, the locations of all the conducting ions are not necessarily
in the regular periodic potential wells of the lattice. Therefore,
in a cooperative motion of ions with a fixed interionic distance,
all the ions do not follow the path in phase with the period of
the potential. In the Fig. (1.2) the relation is shown schematically
for two ions where one ion sits in a potential well while the
neighbouring ion sits on top of the potential barrier. If these
two ions move keeping the fixed interionic distance, a situation
arises in which one ion is moving up the potential barrier while
the other ion is moving down. As a result, the height of the
potential barrier for the cooperative motion is cancelled out.

An interesting model for fast ionic conductors proposed
by Rice and Roth (1972) which resembles closely that of semi-
conductors. The model is based on the hypothesis that there exists
in the ionic conductor an energy gap E_o above which ions of mass M,
belonging to the conducting species, can be thermally excited from
localized ionic states to free-ion-like states in which an ion
propagates throughout the solid with a velocity v_m and energy
$E_m = (1/2) M v_m^2$. To account for the interaction with the rest
of the solid, a finite time T_m for such an excited free ion-ion-
like state is further introduced. Then, based on the Boltzmann
transport equation, simple expressions can be derived for the
ionic conductivity σ .

In the low temperature limit in which $E_O/kT \gg 1$, the result for the ionic conductivity becomes

$$\sigma = (1/3)\ (Ze)^2/(kT)\ n\ v_O l_O \cdot exp\ (-E_O/kT) \qquad (1.6)$$

where n is the density of potentially mobile ions and E_O, v_O, $l_O = v_O T_O$ characterize the free-ion-like state at the energy gap E_O. This expression can be compared with that of the usual hopping model,

$$\sigma = (1/3)\ (Ze)^2/(kT)\ nd^2\ v_O\ exp\ (-E_a/kT) \qquad (1.7)$$

Both equations become identical if E_O is identified with u, the mean free path l_O with d and the inverse life time $1/T_O$ with v_O. Because of the relation

$$v_O = \sqrt{2E_O\ /\ M} \qquad (1.8)$$

σ in the Rice and Roth Eq. can be determined by two adjustable parameters E_O and T_O which can be determined empirically with the knowledge of Z, n and M. It is claimed that l_O and v_O for this approach have clearer physical meaning than obscure quantities like d and v_O in terms of the hopping model in the case of liquid-like motion in fast ionic conductors.

1.4 DISPERSED SOLID ELECTROLYTE SYSTEM :

The ionic conductivity enhancement due to dispersion of inert alumina particles in a LiI matrix[Liang (1973,1974)] or in a CuCl matrix[Jow and Wagner (1979)] has been investigated. The possible mechanisms of enhanced conductivity are discussed from

the point of view of existing theories related to the mixing of
two materials.

1.4.1 Classical Theory :

Maxwell and Raleigh have calculated the conductivity of
a two-phase mechanical mixture in the terms of the bulk conduct-
ivities of the individual phases. They did not consider the effects
due to an electrical double layer at the interface of the coexisting
phases. Therefore according to their theory the conductivity of
.CuCl (Al_2O_3) electrolytes should not be larger than pure CuCl.

Lord Rayleigh (1892) visualised the system as consisting of
cylindrical obstacles which are arranged in rectangular order.
By the principle of superposition the conductivity of the interrupted
medium for a current in any direction can be deduced from its conduct-
ivities in three principal directions. Since conduction parallel
to the axes of the cylinders presents nothing special for consi-
deration, we may limit our attention to conduction parallel to one
of the sides $(\mathcal{X})$ of the rectangular structure. In this case lines
parallel to $\mathcal{X}$, symmetrically situated between the cylinders, such
as AD, BC are lines of flow, and the perpendicular lines AB,CD
are equipotential Fig. (1.3d)/. (p. 24) Using rigorous mathematical relations
it was proved that if a medium, otherwise uniform, be obstructed
by rigid cylinders occupying a moderate fraction of the whole
space, the velocity in the direction parallel to the cylinders
is unaltered.

1.4.2 Classical Doping Theory :

It is conceivable that by the dissolution of insulating particles (e.g., Al_2O_3) in an ionic solid (e.g., CuCl), copper vacancies are created as follows.

$$Al_2O_3 = 2Al_{Cu}^{\bullet\bullet} + V_{Cu}' + 3O_{Cl}'$$

If this were the mechanism for the conductivity enhancement, one would expect that a few mole percent of alumina would be sufficient to reach a concentration of vacancies required to attain an increase of one to two orders of magnitude in the conductivity. Since the solubility of alumina in cuprous chloride was not detectable and the experimental results showed that about 20 m/o alumina with no dissolution was necessary to attain a two orders of magnitude increase in conductivity, the classical doping theory cannot be used to explain the conductivity enhancement in the dispersed phase solid electrolytes such as CuCl (Al_2O_3), AgI (Al_2O_3) etc.

1.4.3 Wagner's Model on Semiconductors Containing Inclusions of Another Phase :

Wagner (1957) applied the concept of electrical double layer at the interface of a two phase mixture to calculate the electrical conductivity of metal oxide, MO_x, involving inclusion of metal, M, particles as a second phase. He considered the cases where the electronic concentration, n , is everywhere much greater than the concentration of electrons and other charged defects in the metal oxides free of inclusions. The electron

concentration n_2, at $r = r_2$ i.e. at an equidistant position between two dispersed particles, was chosen as a parameter for calculating the electron concentration, the electron concentration, n_1, at $r = r_1$ i.e. at the surface of the dispersed particle of radius r_1. From the condition of the constancy of the electrochemical potential of the electronic carriers the space charge density is given as,

$$\rho = -ne = -n_2 \exp (e \emptyset/kT) \tag{1.9}$$

where $\emptyset$ satisfies poisson's equation.

$$^2\emptyset = \frac{d^2\emptyset}{dr^2} + \frac{2}{r} \frac{d\emptyset}{dr} = \frac{-4\pi}{E} \text{ for } r_1 < r < r_2 \tag{1.10}$$

with following boundary conditions

$$\emptyset = 0 \qquad \text{at } r = r_2$$
$$d\emptyset/d_r = 0 \qquad \text{at } r = r_2 \tag{1.11}$$

and E is the dielectric constant of metal oxide.

The numerically estimated value of n_2 is given as

$$n_2 = \frac{(0.28)\ (1.1)}{(5.63)^{1/3}} \left(\frac{g\ ekT}{e^2} \right) \frac{V_v}{r_1^2} \tag{1.12}$$

$$\text{for } n_1 \gg n_2 \quad , \quad r_2 \gg r_1$$

where g is a value which depends on the ratio n_1/n_2, and V_v is the volume fraction of the dispersed second phase.

By disregarding the conduction contribution from the

higher electron concentration surrounding the dispersed particles,
the electrical conductivity of the two phase mixture is expressed
as,

$$\sigma = n_2 e\mu \ \frac{V_v}{r_1^2} \quad \text{for } n_1 \gg n_2, \ r_2 \gg r_1 \qquad (1.13)$$

some of the experimental results including those on CuCl (Al_2O_3)
system were found to be inconsistent with Wagner's theory. This
may be due to two reasons.

First, in his system, the electronic charge carriers of
which there is only one kind and the concentration of the electronic
carriers, n_2 in the bulk depend on the properties of the dispersed
second phase particles. But in CuCl (Al_2O_3) system, there are two
kinds of ionic charge carriers (Cu vacancies and Cu interstitials)
and the concentration of the charge carriers in the bulk [at
a distance remote from the dispersed insulator particles]. Second,
the higher conduction surrounding the dispersed particles was
disregarded by Wagners' system which was reasonable only when the
volume fraction of the dispersed second phase particles was very
small. However, in CuCl (Al_2O_3) system, we studied a system which
contained a large amount of second phase particles.

1.4.4 Jow and Wagner (Space-Charge-Layer) Model:

A pure ionic crystal in thermal equilibrium possesses a
charged surface and a region of space charge of the opposite sign
adjacent to the surface as a result of the difference in the free
energies of the formation of the defects. This was first noted

by Frenkel. Lehovec (1953) discussed the importance of the space charge region near the surface on ionic conduction, diffusion, photoelectric effect and photographic effect. Kliewer and Koehler (1965) have calculated the defect distribution near the surface in both pure monovalent crystals and crystals containing divalent cationic impurities for Schottky disorder. Kliewer (1966) has calculated those for Frenkel disorder. Since cuprous chloride is a crystal possessing Frenkel disorder consisting of interstitial copper ions and copper vacancies, Kliewer's result on a crystal of Frenkel disorder of finite length in x direction but of infinite length in y .d z directions is stated below. The concentration of copper interstitials, $n_i(x)$ or vacancies $n_v(x)$, is dependent on the space-charge potential $\phi(x)$ by the relations,

$$n_v = N \exp\left[- (F^V - e\phi) / kT \right] \tag{1.14}$$

$$n_I \doteq 2N \exp\left[-(F^I + e\phi) kT \right] \tag{1.15}$$

where N is the number of CuCl ion-pairs per unit volume F^V is the free energy of formation of a vacancy and F^I is the free energy of formation of an interstitial, and the potential $\phi(x)$ is the solution of Poisson's equation,

$$\frac{d^2 \phi(x)}{d x^2} = \frac{4 \pi \, \rho(x)}{E} \tag{1.16}$$

where $\rho(x) = e \left\{ n_I(x) - n_v(x) \right\}$ is the change density and E is the static dielectric constant. Substitution of the solution $\phi(x)$ into (1.14 and (1.15) gives the complete dependence of the defect

concentration on position, x. The space-charge layer extends
a distance roughly equal to λ which is expressed as follows,

$$\lambda = \left\{ \frac{8\pi Ne^2}{EkT} \quad \exp\left[e\phi_{\infty} - F^V)/kT\right] \right\}^{-1/2} \qquad (1.17)$$

where ϕ , the potential difference between the surface and
the bulk, is given by

$$\phi_{\infty} = \frac{1}{2e} \left(F^V - F^I + kT \ln 2 \right)$$

λ can be expressed as

$$\lambda = \left\{ \frac{8\pi e^2}{ekT} \; n_v(\infty) \right\}^{-1/2} = \frac{8\pi e^2}{EkT} \; n_I(\infty) \qquad^{-1/2} \quad (1.1$$

where $n_v(\infty)$ and $n_I(\infty)$ are the equilibrium defect concentrations
of copper vacancies and copper interstitials in the bulk, respecti-
vely.

Since the defect concentration near the surface of an
ionic solid is different from that in the bulk, the conductivity
near the surface differs from that in the bulk as well. If we
consider the interfaces between CuCl and alumina particles at
the surface of cuprous chloride and consider the space-charge
layer around the alumina particles surfaces as a possible mechanism
for the conductivity enhancement in the CuCl (Al_2O_3) system, then
the space-change layer around grain boundaries should also be
included.
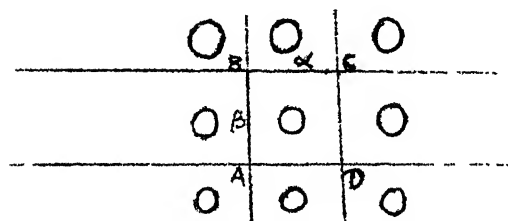
Fig 1.3 (d)

Since the specimens of CuCl (Al_2O_3) have about the same grain sizes which are much larger than the particles sizes of alumina, the contribution of grain boundaries to the conductivity enhancement is much smaller than that of the surfaces of the alumina particles.

Consider the conduction in a volume of $(4/3)\pi r_4^3$ containing one single dispersed alumina particle of radius r_1 and r_2 r_1 as shown in the Fig. (1.3). This conduction can be expressed as

$$\sigma = \sigma_o + \triangle\sigma = \sum_i n_i (\sigma) \, e\mu_i +$$

$$\sum_i \mu_i e \left\{ \frac{\int_{r_1}^{r_2}\int_0^{\pi_2}\int_0^{2\pi} [n_i(r)-n_i(\infty)] \, r^2 dr \sin\theta d\theta d\varnothing}{\int_{r_1}^{r_2}\int_0^{\pi/2}\int_0^{2\pi} r^2 dr \sin\theta d\theta d\varnothing} \right\} \quad (1.19)$$

where σ_o is the ionic conduction of the halide matrix in the bulk. In Eq. (1.19), σ denotes the extra conduction due to the space-charge layer, and the summation is the sum over the different charged defects. The subscript i denotes the ith defect species, here we only consider the M^+ interstitials and the M^+ vacancies. μ_i is the mobility of the defects which is assumed to be independent of position. Therefore, σ can be calculated from the known defect distribution.

If we assume that the space-charge layer is smaller than the radius of the alumina particle, i.e. $\lambda < r_1$, and the excess defect concentration near the surface can be represented by an
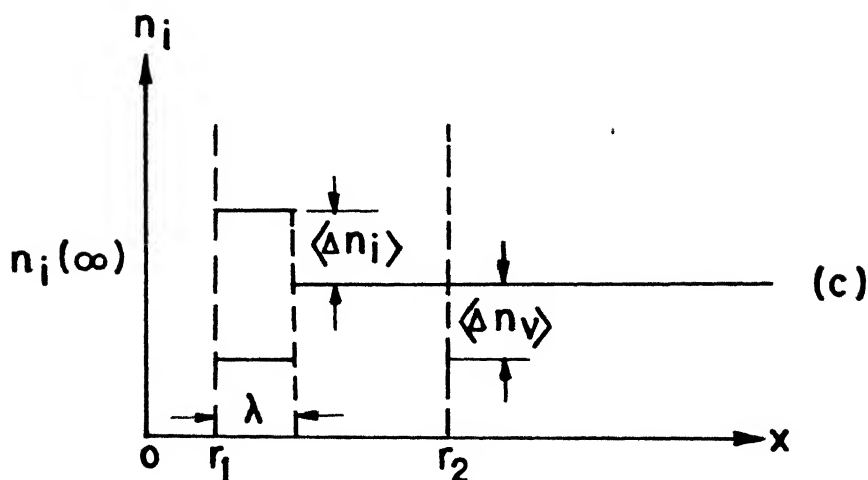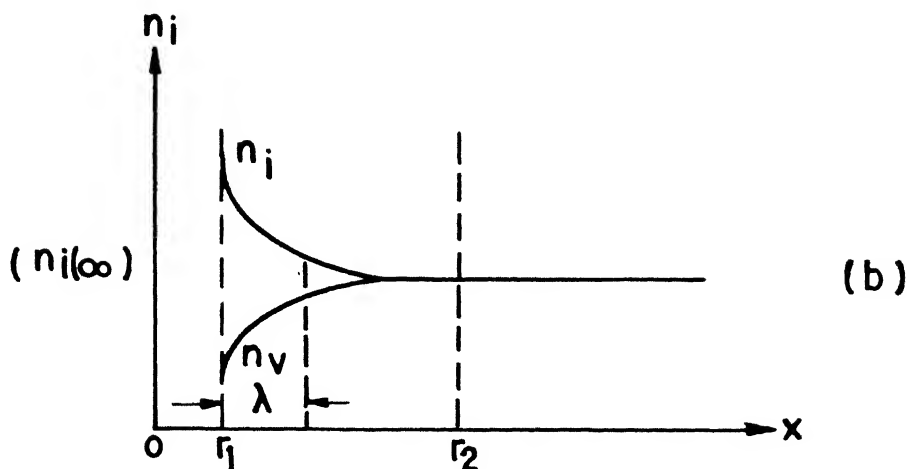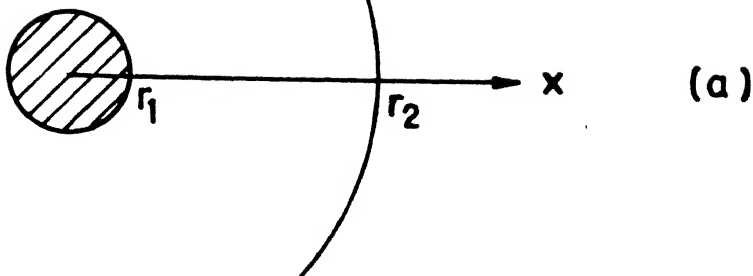
Fig. 1.3   (a) Schematic cross sectional view of a single alumina
                particle of radius r_1 in CuCl matrix. $2r_2$ is the
                average distance between two alumina particles.

           (b) Sketch of the defect concentration along the x-axis,
                where $F_I < F_V$ is assumed.

           (c) Sketch of the average excess charge density (Δn_i) i
                the space-charge layer along the x-axis.

average excess charge density n_I , in the space-charge layer of a thickness λ , then Equ. (1.19) can be expressed as

$$\sigma \sim 1 \ \sum_i e\mu_i \langle \Delta n_i \rangle \ \frac{4\pi r_1^2 \lambda}{\frac{4\pi}{3}(r_2^3 - r_1^3)} \qquad (1.20)$$

or

$$\sigma = 3 \sum_i e\mu_i \langle \Delta n_i \rangle \ \frac{(\frac{r_1}{r_2})^3}{[- (\frac{r_1}{r_2})^3]} \qquad (1.21)$$

The ratio of r_1/r_2 is a function of volume fraction of the dispersed second phase.

If we further assume that $r_2 \gg r_1$, then $(r_1/r_2)^3 = V_v$ and equation (1.21) can be written as,

$$\sigma = 3 \sum_i e\mu_i \langle \Delta n_i \rangle \ \lambda . (\frac{1}{r_1}) (\frac{V_v}{1-V_v}) \text{ where } r_2 \gg r_1 \quad (1.22)$$

where μ_i, $\langle \Delta n_i \rangle$ and λ are functions of temperature. At a definite temperature, the excess conductivity $\Delta \sigma$ is proportional to $(1/r_1) \cdot (V_v)/(1-V_v)$ for the cases where $r_2 \gg r_1$.

Although Eq. (1.22) does not give a quantitative model for the experimental result, it does provide a qualitative explanation.

The fact that the conductivity enhancement is large at low temperatures and small at high temperatures, can be explained by Equation (1.22) , since the thickness of the space-charge layer λ

decreases with increasing temperatures. The data show that the maximum enhancement in conductivity occurs at lower temperatures. As the temperature increases, those defects introduced by charged surfaces of the dispersed particles play a smaller role in ionic transport.

For a given temperature, the conductivity attains a maximum value at a critical mole fraction of added second phase, The decrease in conductivity for additions of more second phase is due to the fact that the volume occupied by the insulator particles becomes a large fraction of the total. Moreover, as the dispersed particles approach each other, there should be an optimum distance between the particles for maximum enhancement.

1.5 APPLICATIONS OF HALOGENIDE SOLID ELECTROLYTES :

Since the main use of solid electrolytes is in electrochemical devices, it is desirable to first discuss the electrochemical devices.

1.5.1 Electrochemical Devices:

Electrochemical devices differ from electronic devices in that the passage of current requires the motion and transfer of both ions and electrons. They are thus not passive in a mechanical sense and whenever an electrochemical device is incorporated into an electronic circuit, it will inevitably emerge as the weakest link . This is particularly true for multicomponent liquid electrolyte systems because of the large number of charge

transfer or faradaic reactions which are possible. In a system based on an aqueous electrolyte one must thus take into account not only reactions associated with an active oxidant or reductant, but also the numerous electrode reactions of the H_3O^+ or OH^- ions. The practicality of any electrochemical device concept which relies on the use of an aqueous electrolyte is often, therefore, a compromise between the needs for acceptable materials for long term stability and the obtaining of satisfactory performance.

The ideal electrolyte as reported by Geller (1977) should:

(a) be both chemically and physically invariant

(b) provide a path for ionic transport, and a barrier to electronic transport.

(c) serve as a mechanical separator for the electrodes.

Solid electrolytes go a long way towards fulfilling these requirements. The number of materials having sufficient low temperature ionic conductivity to permit their use in practical devices is largely restricted to the Ag^+ ion conducting families and to a lesser extent some Li^+ ion conductors. The widest range of devices demonstrated to date has been based on Ag^+ ion electrolytes and in particular $RbAg_4I_5$. The greatest commercial interest today, however, is in Li^+ ion conductors which are beginning to find wide application in high energy density batteries for use in specialized applications such as cardiac pace makers.

1.5.2 Device Concepts:

Four main device concepts utilizing solid electrolytes will be discussed, namely:

    (i)   Primary batteries

   (ii)   Capacitors

  (iii)   Rechargeable batteries

   (iv)   Coulometers and timers

(i)   Primary Batteries:

Although Ag^+ solid electrolytes have been widely used in primary batteries the discussion here will be limited to Li^+ solid state batteries.

(a) Lithium-Metal Salt Solid State Batteries:

Liang et al (1973) have investigated solid state batteries based upon lithium anodes and various nonvolatile, metal salts as the cathode. The use of elemental iodine or polyiodide compounds as a cathode has the disadvantages associated with the volatility of iodine, the self-discharge and material corrosion problems are caused primarily by the diffusion of the reactive iodine. These specific problems are avoided by the use of solid, nonvolatile salts as cathodes in high voltage cells.

The Cell Li/LiI/AgI has an open circuit voltage of 2.1V corresponding to the reaction

$$Li + AgI \rightarrow LiI + Ag$$

These cells were restricted to very low drain rates (($10\mu A/Cm^2$) because of ohmic polarization losses. In addition the system was unstable because of interdiffusion of Li^+ and Ag^+ ions, resulting in self-discharge losses.

The use of the more conducting LiI (Al_2O_3) electrolyte caused a practical energy density of 0.5 Wh/Cm^3 at low current densities.

Such batteries are stable and exhibit no capacity loss during storage at elevated temperatures. This system is possibly the most stable active primary battery available, provided it is hermetically sealed. Because of the reactivity of the Li with H_2O, N_2 and O_2 and the LiI with H_2O, the cells are fabricated in H_e dry boxes with the concentration of H_2O and O_2 being maintained below 15 PPM.

(b) Lithium-Halogen Solid Electrolyte Batteries:

The battery described previously is based upon a pellet type of cell construction wherein anode and cathode disks are separated by a dense electrolyte disk of 0.02 to 0.10 cm thickness. The electrolyte is formed during fabrication as an integral layer separating the electrodes . Lithium-halogen batteries have been developed wherein the lithium halide electrolyte is formed in situ by the direct combination of the active electrode components. Cells of this type have been reported for Li/I_2 and Li/Br_2.

Pure iodine does not have adequate electronic conductivity to sustain discharge in a cell $Li/LiI/I_2$. However, by combining the I_2 with poly-2-vinylpyridine one obtains a charge-transfer-complex with an electrical conductivity of 10^{-3} [Ωcm]$^{-1}$

The Li/I_2 cell has been under development for several years and is presently finding sucessful application as the power

source for cardiac pacemakers. The uniqueness of this battery is closely related to the composition of the cathode, an iodine poly-2-vinypyridine change transfer complex (CTC) serves as the cathode. When the CTC contacts the Li anode, it immediately formation a thin film of LiI at the interface of the electrodes. The cell will promptly exhibit a cell voltage of 2.80, in good agreement with the value 2.796V calculated from the Gibbs free energy of form for LiI. The cell reaction may be written as:

$$2Li + I_2 \rightarrow 2LiI$$
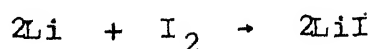
Discharge of the Li/I_2-CTC cell results in the formation of resistive LiI, and the battery impedance increases. The cell is, therefore, restricted to low current densities and moderate temperatures. It is ideally suited for the pacemaker application at 37°C and current densities of 1-10 $\mu A/cm^2$, under these conditions energy densities as high as 0.8 Wh/Cm^3 have been projected.

Li/Br_2-CTC cells have also been developed. The cell exhibits a voltage of 3.50V. The more energetic bromine cell is projected to deliver 1.25 Wh/cm^3 at low rates.

The lithium/halogen cells represent a significant new type of power source. The Li/I_2-CTC batteries are extremely useful in powering cardiac pacemakers efficiently and with high reliability.

(ii) Rechargeable Batteries:

In many solid state applications, failure due to

volatility of semiconductor systems during transient or long term power failures may be in some cases inconvenient, in others hazardous or expensive. There is thus a need for a solid state, wide temperature energy store to be compatible with rugged, high reliability semiconductor electronic systems. As a source of secondary power, conventional secondary batteries have generally proven to be incompatible with semiconductor electronics. A useful device for these applications is a capacitive type energy store with all the environmental and shelf-like characteristics of a good quality capacitor, but at the same time an energy storage capability approaching that of a secondary battery.

In addition to standby power there are other potential applications, eg. where it is necessary to minimize power supply requirements such as in a system employing a low current power source which must have an occasional low duty cycle, higher current output. A typical application is a telemetry system with occasional operating periods. Power could be obtained from solar cells or similar low power devices and stored in a rechargeable battery for use during an occasional data transmission.

The capacitor described below can conceptually be employed in such applications but applicability is limited by its low energy storage capability and it is desirable that this be described considerably

(iii) Electrochemical Capacitor:

The capacitance in an electrochemical capacitor is dirived from the electrical double layer that exists at an electrode/electrolyte interface. The value of capacitance that can be achieved are thus intrinsically higher than those in which a dielectric layer is employed and this constitutes their main advantage over dielectric types i.e. much higher capacitance per unit volume.

The basis for electrochemical capacitors utilizing $RbAg_4I_5$ is the ideally polarizable carbon electrode. The double layer capaci at a carbon/$RbAg_4I_5$ interface falls in the range $20-40\mu F/cm^2$. In its polar form it is represented as

$$Ag/RbAg_4I_5/C$$
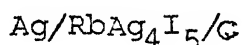
only the carbon electrode is capacitive. Silver behaves as an ideall non-polarizable electrode, and it can be considered to have infinite capacity, during charging.The voltage change of the carbon electrode is nearly linear between 0 and 0.45V, and the integral capacity (C_{int}) is given by

$$C_{int} = \frac{idt}{dE}$$

During discharge, silver metal is oxidised to Ag^+ ions and the double layer at the carbon electrode is discharged. Devices of different capacity can be fabricated simply by varying the weight of the carbon electrode, which consists of a carbon/$RbAg_4I_5$ mixture.

The high energy storage capability of the solid state electrochemical capacitor coupled with very low leakage current makes it an ideal device for use with operational amplifiers. Because of the low voltage at which charge is stored, the device can be charged from a voltage source through a resistor at what approximates very closely a constant current charge condition. Thus, 5V and above power supply operation is totally acceptable. This can be done by connecting several devices in series to provide a higher operating voltage.

(iv) Solid Electrolyte Coulometers (Timers)

Coulometry based on the electrodeposition of a metal and subsequent anodic stripping from an inert substrate has long been a viable electroanalytical tool. The basic requirement is that the coulombic efficiency be unity or close to unity. Liquid electrolyte systems, usually based on silver, have a long record of satisfactory use in such applications under normal ambient conditions. However, at extremes of temperature or where the application demands unusual ruggedness, reliability and accuracy, it is desirable not to rely on a liquid electrolyte system. Typical instances are when the device must be incorporated as an integral component in microelectronic circuitry or be subjected to unusual stress as in certain military use e.g. timing devices for ordinance

Basically the conlometer consists of a material which is produced at an indicator (inert) electrode when the cell is 'set' or accumulating 'charge' . Subsequently, the amount of this material

is determined by weight, volume or electrical measurements. Most practical timers now use electrical 'readout'. This is accomplished by monitoring the voltage across the cell, and when the indicator electrode is completely 'stripped' a large voltage occurs. A recording of voltage versus time is referred to as the 'Discharge' or 'stripping' curve and the final voltage rise when stripping is complete as the 'cut off'. If one utilizes a Ag^+ conducting solid electrolyte the cell would operate in the following fashion:

Cell	Ag	AgX	M
'Charge' or 'Set'	$Ag \rightarrow Ag^+ + e^-$		$Ag^+ + e^- \rightarrow Ag$
'Discharge' or S	$Ag^+ + e^- \rightarrow Ag$		$Ag \rightarrow Ag^+ + e^-$
'cut off' or 'end	$Ag^+ + e^- \rightarrow Ag$		$M + nX^- \rightarrow MX_n + ne^-$
			or $X^- \rightarrow X + e^-$

The primary requirement is that the cell must operate at 100% current efficiency i.e. the number of coulombs necessary to strip the cell equals the number of coloumbs used in the initial setting.

--

CHAPTER - 2

EXPERIMENTAL DETAILS

The present investigation was aimed at developing a solid electrolyte based on LiBr containing a dispersion of fine Al_2O_3 particles. The electrical conductivity of polycrystalline LiBr has been reported to be $1.6 \times 10^{-9} \, \Omega^{-1} cm^{-1}$ at room temperature. The experimental effort involved the preparation of samples and pellets, the designing and fabrication of sample holder, furnace etc. measurement and analysis of the complex .impedance as a function of the concentration of Al_2O_3 particles in LiBr and temperature. The study of microstructure was done using Scanning Electron Microscopy.

2.1 Starting Materials and Preparation :

Lithium Bromide (anhydrous) of 98 ÷ % purity was obtained from ALFA Products, Thiokol/Ventron Division.

Physical Properties of LiBr

Molecular Weight - 86.85

Crystalline Properties - Cubic, Deliaquescent

Refractive Index - 1.784

Density - 3.464 g/cc

Melting point - 550°C

Boiling Point - 1 265°C

Al_2O_3 was obtained from Aluminium Corporation of America. (ALCOA) .

Physical Properties of γ-Al$_2$O$_3$

Molecular Weight - 101.96

Crystalline Form - Microscopic Crystalline

Refractive Index - 1.7

Density - 3.5 - 3.9 g/cc

Melting Point - Transition to (2015 $\pm$ 15°C)

LiBr and Al$_2$O$_3$ were taken in proper proportion, mixed thoroughly in an agate mortar and pestle followed by pelletization (as discussed in the next section) at   4 ton/Cm^2 and heating the compacted mixture at a temperature of 370 $\pm$ 10°C for about 17 hrs. Table 2.1 gives the preparational details of the samples of various compositions. The pellets so obtained were crushed repowderized and repelletized.

2.2 Preparation of Pellets :

The fine powder of each composition was transferred to a stainless-steel die which is shown in Fig. 2.1. After levelling the powder by means of the die-piston, the whole assembly was placed in a hand-operated hydraulic press. The pressure used in all cases was 4 ton/cm^2. The piston diameter fixed the diameter of the pellets at 1.1 cm, while the thickness of the pellets usually ranged between 0.3 and 0.5 cm. Thorough cleaning of the die with acetone, before and after use was observed as a usual practice. Pellets were kept in small specimen bottles which in turn were stored in a vacuum desiccator.

2.3 The Experimental Set Up :

The electrical conductivity measurements as a function of
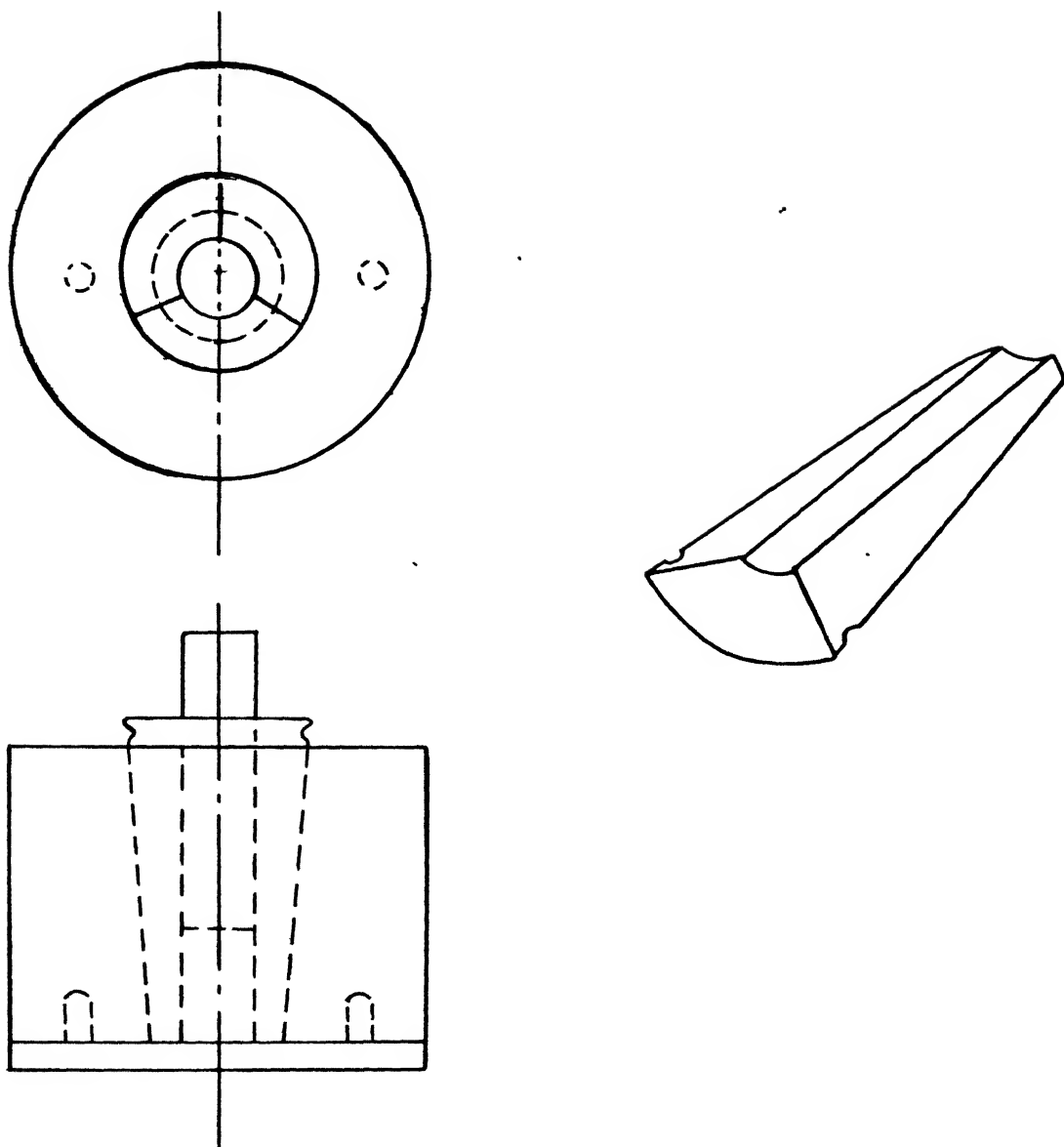
FIG. 2·1 STAINLESS STEEL DIE FOR MAKING PELLETS

Table 2.1

Details of Preparation of Samples

Composition	Wt. of LiBr (Gm)	Wt. of Al_2O_3 (gm)	Pelleti-zation pressure ton/cm^2	Temperature and duration of heating of pellets for homo-genization	
				Temp $\pm$ 10°C	Time (Hrs.)
LiBr	2.00	O	4 .	370	17
LiBr + 5m/o Al_2O_3	1.8849	0.1151	4	370	17
LiBr+10m/o Al_2O_3	1.7715	0.2285	4	370	17
LiBr+15m/o Al_2O_3	1.6594	0.3406	4	370	17
LiBr+20m/o Al_2O_3	1.5592	0.4506	4	370	17
LiBr+25m/o Al_2O_3	1.4420	0.5580	4	370	17

temperature requires a furnace, a sample holder, a temperature
controller and an impedance bridge. The sample holder and the
furnace were designed and fabricated locally as discussed below:

2.3.1   Furnace :

Kanthal wire of 2mm $\underset{\diagup}{\text{(dia)}}$ was wound inductively and uniformly
at the rate of about 10 turns per inch on a mullite tube (18″ in.
length, $2\frac{1}{4}$ in. in diameter). The total resistance of the heating
element was 34 Ohms. A high temperature current was applied
directly over the windings to a thickness of about 1/2″, and then
allowed to dry at room temperature for a few days and later a small
current was passed to further dry up the cement.

The Mullite tube wound with Kanthal wire was housed in a
cylindrical aluminium construction which was open at both ends.
Two asbestos and aluminium circular plates were used to cover the
two flat ends of the furnace and were fixed in place with screws.
The space between the mullite tube and aluminium enclosure was filled
with MgO powder to minimize the heat loss.

2.3.2 The Sample Holder

The sample holder in this case was specially equipped
to take measurements under vacuum. Fig. 2.2 shows the schematic
diagram of the sample holder. It consists of an inner body that
is enclosed by a quartz tube that can be evacuated. This inner
body comprises of three identical lava discs. The outstanding
qualities of lava material are that it is machinable, can withstand
high temperatures (upto 1400°C) and a good electrical insulator.

Sectional view of the insulating
lava disc
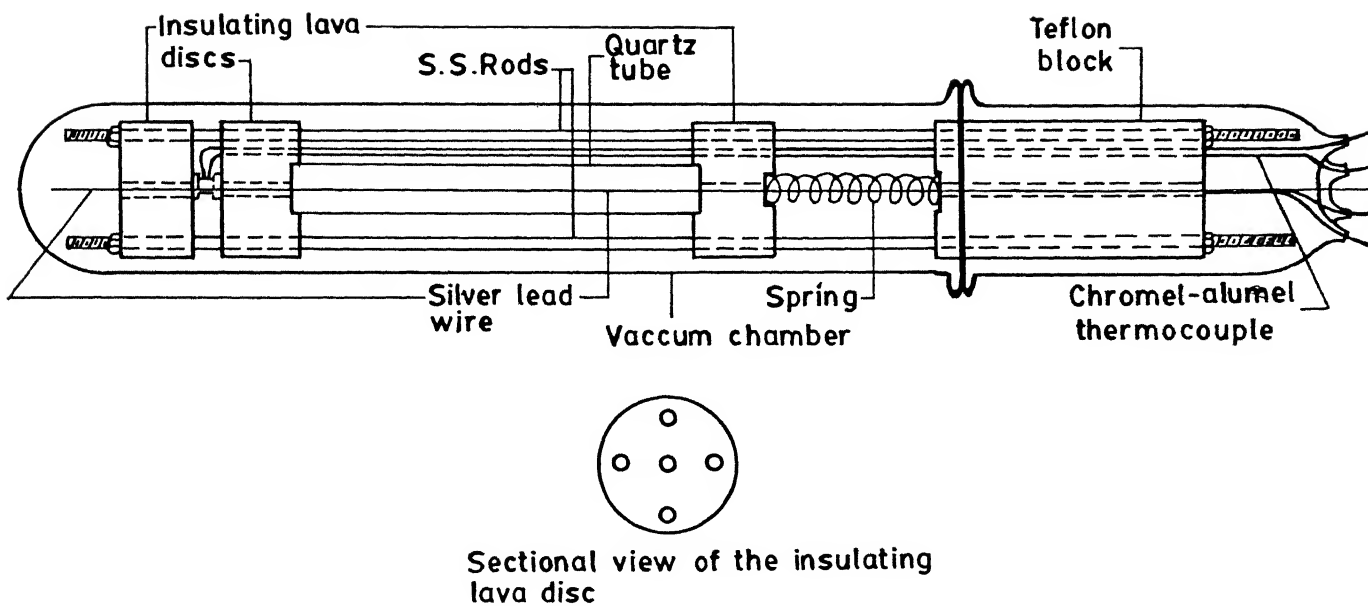
FIG.2·2 SAMPLE HOLDER FOR THE ELECTRICAL CONDUCTIVITY MEASUREMENT

Each lava disc has five parallel through holes in it. The four holes located symmetrically around the circumference are each of 4 mm. diameter while the hole at the center of the disc was different in the three pieces according to the need in the design. Two of the holes near the circumference were used by the two stainless steel rods which acted as the support in the holder. The third hole was used for taking out the thermocouple-leads through double holed thin alumina rod, while the fourth hole takes care of one of the silver leads brazed to the lower platinum electrode. The other silver lead-wire brazed to the upper platinum electrode was passed through the quartz tube, spring and eventually comes through the central hole of the teflon block. The spring located outside the furnace is used to exert a sufficient and uniform pressure required for point to point contact between the electrodes and the sample.

The lava discs, after machining were heated slowly to 1000°C and kept at that temperature for 2 hours before cooling inside the furnace. This kind of heat treatment is necessary to harden the lava disc and also to remove any moisture content. The effert of the latter is to increase the resistivity of the disc significantly

2.3.3 Measurements :

This work involved extensive electrical conductivity measurements. A block diagram of the set up used is given in Fig. 2.3.

The temperature inside the furnace was controlled using an Indotherm Temperature Controller (Model 401). A

Impedance bridge	Furnace & Sample holder	Temp. controller	Microvolt DMM

H
L

E
E
+
−

TC
+
−

H
G

Silver lead wires

Chromel - alumel
Thermocouple
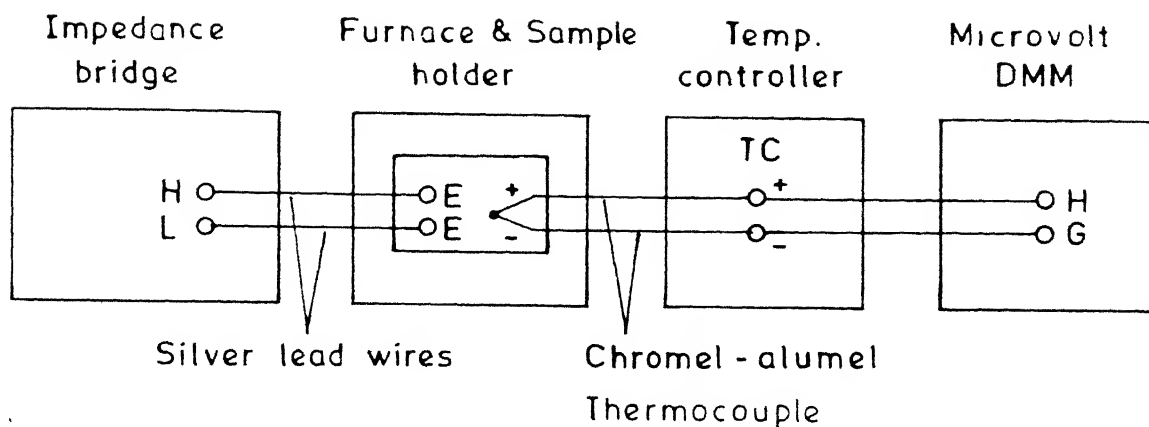
FIG. 2·3 Block diagram connections for electrical conductivity measurements.

Keithley microvolt DMM was used to measure the thermocouple voltage and hence temperature. HP-4192A low frequency Impedance Analyzer was used for impedance measurements at various temperatures. This instrument has a wide frequency range of 5Hz to 13MHz.

To measure the impedance of the samples, the flat surfaces of the cylindrical pellets were first polished on different grades of fine polishing papers to remove the surface contaminations and to obtain parallel and smooth surfaces. Two stainless steel discs of same diameter as the pellet and about 1.5 mm thickness were placed between the pellet and the platinum electrode for proper contact. The stainless steel discs were also polished on fine graded emery paper before each set of measurements. Having loaded the sample in the holder, the tip of the chromel-alumel thermocouple wire was placed as close to the sample as possible to measure as well as control the temperature of the sample. The vacuum quartz tube was sealed at one end with araldite. The sample holder was then put inside the furnace which was closed at one end to ensure a steady state to be reached rapidly. The samples were annealed at roughly two-third of the melting point of LiBr, i.e. 550K for about 6 hrs to relieve the sample of the stresses introduced during the pelletization, homogenize the charge carriers and reduce the grain boundaries. The temperature was then raised to 400°C and the impedance measurements were done in the cooling cycle.

2. 4 Complex Impedance Analysis :

The HP- 4192A Low Frequency Impedance Analyser can accurately

measure the impedance parameters of a component or a circuit at various frequencies, test signal levels and dc bias levels found in actual-real world operation. The ranges available are:

(1)   Measuring frequency : 5Hz to 12 MHz

(2)   OSC Level : 5mV rms to 1.1 V rms

(3)   DC bias voltage: −35V to +35V

Frequency and bias can be automatically or manually swept, full range, in either direction. DSC level can also be swept (manual only) at 1 mV steps (5mV steps at levels above 100mV).

For connecting the sample to be tested, the HP-4192A employs measurement terminals in a four terminal pair configuration which has a significant measuring advantage for component parameter requiring high accuracy in the high frequency region. Generally, any mutual inductance, interference of the measurement signals, and unwanted residual factors in the connection method which are incidental to ordinary terminal methods significantly affect the measurement at a high frequency. The four terminal pair configuration measurement permits easy, stable and accurate measurements and avoids the measurement limitations inherent in such effects. Fig. 2.4 shows the four terminal pair measurement principle. The unknown terminals consist of four connectors: High current (H_{CUR}), High potential (H_{POT}) Low potential (L_{POT}) and low current (L_{CUR}). The purpose of the current terminals is to cause a measurement signal current to flow through the device under test (DUT) or sample. The potential terminals are for detecting the voltage
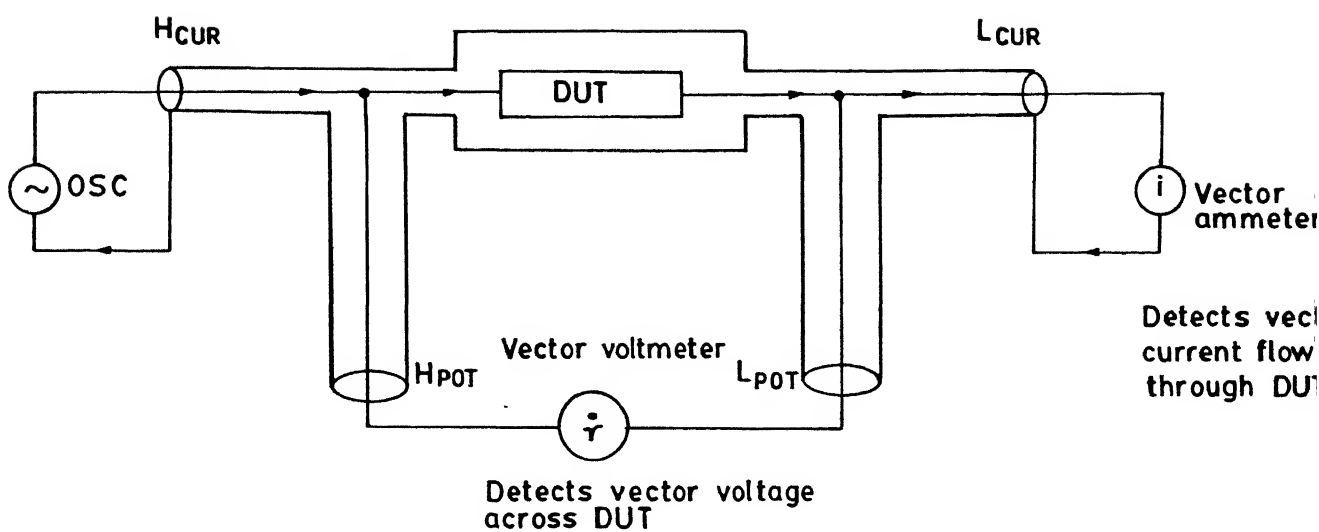
FIG. 2·4   FOUR TERMINAL PAIR MEASUREMENT PRINCIPLE

drop across the sample. The high side represents the drive potential with reference to low side potential drawn from the internal measurement signal source. The main principle is that the measurement signal current does not develop an inductive magnetic field and thus the test leads do not contribute additional measurement errors due to self-or mutual- inductance between the individual leads.

However, the four terminal system must be converted to a two terminal configuration at/near to the sample because the sample/ device under test (DUT) has two leads.

The impedance of a component can be expressed in vector representation by a complex number as shown in Fig. 2.5. In such a representation, the effective resistance and effective reactance correspond to the projections of the impedance vector Z θ, that is, the real (R) axis and the imaginary (jX) axis, respectively. When the phase angle, θ, changes both Re and x change in accordance with the above definition. The measurements made by this instrument were then analyzed using complex impedance plots.

2.4.1 Complex Impedance Plots:

Complex impedance plots are useful for determining an appropriate equivalent circuit for a system and for estimating the values of the circuit parameters. The complex impedance $Z(\omega)$ of a system at an applied angular frequency ω may be written as the sum of a resistance $R(\omega)$ and a reactance Xe:

$$Z(\omega) = R(\omega) + j\, Xe\,(\omega)$$
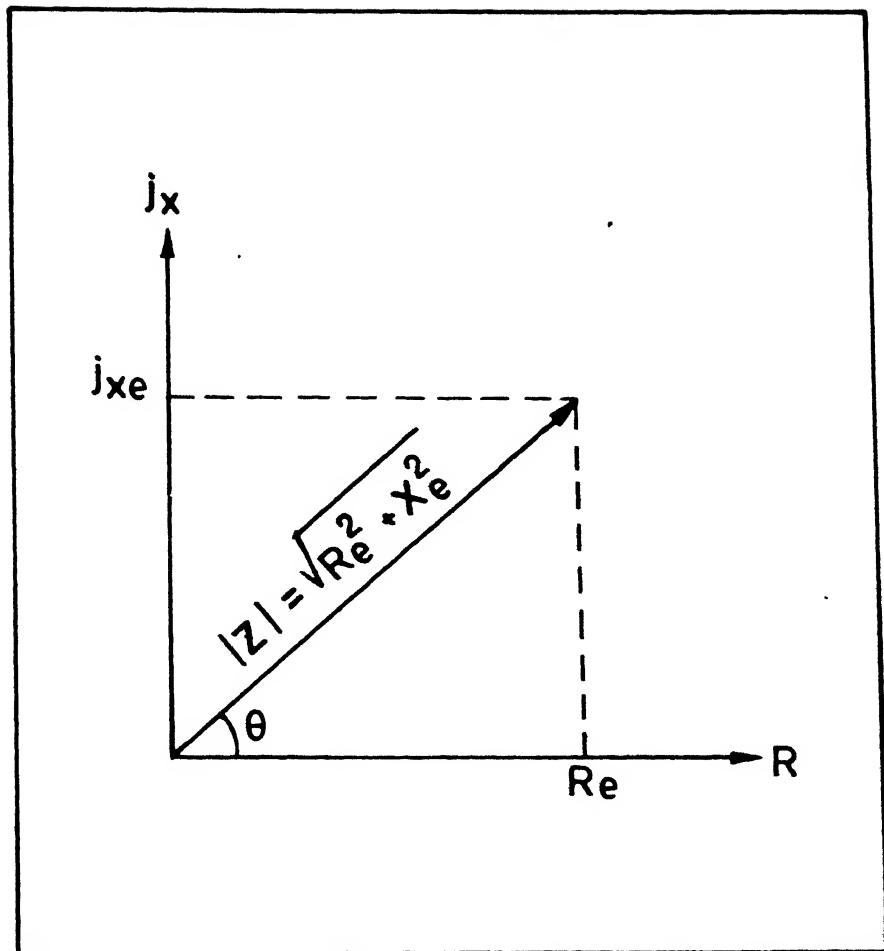
FIG. 2·5 IMPEDANCE VECTOR REPRESENTATION

If one plots the imaginary part of the impedance Vs. the real part i.e. $X_e(\omega)$ Vs $R(\omega)$, the resulting locus shows distinctive features for certain combinations of circuit elements. The method is best illustrated by specific examples of such plots shown in Fig. 3.1 for some simple circuits. Very roughly, one can say that each semi-circular arc corresponds to a " lumped" R-C combination, each quarter circular arc corresponds to a combination of a lumped R and a distributed R-C element. The resistive values can be derived from the circular-arc intercepts on the G-axis, the capacitance values can be derived from expressions involving the frequencies at the peaks of the circular arcs.

2.3.4   Scanning Electron Microscopy (SEM)

The scanning electron microscopy (SEM) is the most powerful tool to study the surface topography and morphology with an unprecedented advantage of depth of field and a capability for studying any surface in its original unaltered state. From the standpoint of actual surface microscopy, the scanning electron microscopy images topographical details with maximum contrast and depth of field by the detection, amplification and display of secondary electrons.

Our primary interest was to study the microstructure of LiBr-Al$_2$O$_3$ composites. The previous studies on the composite solid electrolytes emphasize the role of interfaces between the dispersed particle (e.g. Al$_2$O$_3$) and the host matrix (e.g. LiBr) in the conductivity enhancement. It therefore becomes important

to understand the distribution pattern of the dispersed particles. The SEM study can also yield the size of the particles in the host matrix. It has often been found that the particle size of the dispersed phase does not remain the same as before mixing.

The samples for SEM measurement were prepared by breaking small portions from the pellets (~3mm). The pieces were then mounted on an aluminium stub with Duco Cement and painting silver paint around the edge of the specimen and the stub. Then they were transferred to a vacuum jar and coated with a conducting layer of silver by vacuum deposition. Then the specimens were ready for SEM observations.

Chapter   3

RESULTS   AND   DISCUSSION

The study of the electrical properties of solid electrolytes containing a dispersion of fine insulating particles such as Al_2O_3, SiO_2 etc. has assumed a great significance in recent times primarily because of two reasons. Firstly, the large increase in the ionic conductivity due to the dispersed (second phase) nsulating particles is totally unexpected, in fact according to the classical theories the conductivity of a mixture consisting of two materials should be somewhere between the conductivities of the two individual phases. Contrary to this, the conductivity of the composite solid electrolyte is found to be orders of magnitude higher than the conductivities of either pure phase. Secondly, the composite solid electrolyte have been found exceptionally stable under the hostile battery environments, a very severe condition that many a solid electrolytes do not satisfy. For example LiBr-Al_2O_3, Li_3N etc. are far better solid electrolytes but they are not stable in contact with Li metal anode.

In view of these two facts, namely, (i) the good stability of the composite solid electrolytes in the battery environment and (ii) the anomalously large ionic conductivity, the composite solid electrolytes are being studied very actively all over the world. Liang (1972) was the first to report a conductivity enhancement by about two orders of magnitude in LiI.Al_2O_3 system.

Subsequently, a number of other systems have been examined, $AgI-Al_2O_3$, $AgI-SiO_2$, $AgI-Flyash$ (Shahi and Wagner, 1981). All these studies have established that there is anomalous increase in the conductivity by the dispersed second phase particles. However, there are several discrepancies that have come to the light regarding the role of absorbed water either by the solid electrolyte itself or the dispersoids (e.g. Al_2O_3). the effect of size of the dispersoids, the mechanism responsible for the enhancements etc.

This chapter reports the results on $LiBr-Al_2O_3$ composites with a view to improve the conductivity of $LiBr$, to contribute towards the understanding of the conductivity mechanism in dispersed phase solid electrolytes, to ascertain the role of water, etc. More specifically, this chapter deals with the following measurements and their analysis.

(i) The complex impedance analysis and the determination of the pu
ly resistive part of the specimen.

(ii) The conductivity vs. frequency dependence

(iii) The variation of conductivity with composition

(iv) The variation of conductivity with temperature

(v) Scanning electron microscopy (SEM) studies.

3.1 COMPLEX IMPEDANCE ANALYSIS (CIA) :

The conventional method for electrical characterization of solid electrolytes or for that matter any material is to measure the a.c. conductivity at 1 kHz frequency. While this

method has been in use for a long time and continues to be used even today, it is now well recognized that this method is applicable only when the system under test is purely resistive. Strictly speaking only metallic systems would fall in this category. For other materials including the solid electrolytes, the cell assembly, i.e. the sample + electrode + leads, represents a complex impedance involving resistance and capacitance. The latter arising due to the capacitance between the electrodes and the sample and the capacitance due to grain-boundaries, etc. Thus the unknown sample is like a blackbox consisting of resistance and capacitance in an unknown configuration. Hence, to determine the resistivity/ conductivity of the sample a complex impedance analysis has to be used.

Baurle (1970) was among the pioneers in applying the complex Impedance Analysis for solid electrolyte characterizations. He found the need for a method in which :

(1) The current through the cell is kept very low to avoid irrever-sible electrode changes and heating effects.

(2) A method which is capable of resolving several polarizations occuring in the same specimen.

An obvious solution to these difficulties is to study the impedance of the cell as a function of frequency with low amplitude a.c. but there still remains the awkward problem of analyzing data involving several polarizations which may partially overlap in the frequency domain. Thus, the cell admittance was taken over a wide range of frequencies and then analyzed in the " complex admittance plane".

method has been in use for a long time and continues to be used even today, it is now well recognized that this method is applicable only when the system under test is purely resistive. Strictly speaking only metallic systems would fall in this category. For other materials including the solid electrolytes, the cell assumbly, i.e. the sample + electrode + leads, represents and capaciatnce. The latter arising due to the capacitance between the electrodes and the sample and the capacitance due to the capacitance between the electrodes and the sample and the capacitance due to grain-boundaries, etc. Thus the unknown sample is like a blackbox consisting of resistance and capacitance in an unknown contiguration. Hence, to determine the resistivity/conductivity of the sample. The complex impedance analysis has to be used.

Baurle (1970) was among the pioneers in applying the complex Impedance Analysis for solid electrolyte characterizations. He found the need for a method in which.

(1) The current through the cell is kept very low to avoid irreversible electrode changes and heating effects.

(2) A method which is capable of resolving several polarizations occuring in the same specimen.

An obvious solution to these difficulties is to study the impedance of the cell as a sunction of frequency with low amplitude a.c. but there still remains the awakward problem of analyzing data involving several polarizations which may partially overlap in the frequency domain. Thus, the cell admittance was taken over a wide range of frequencies and then analyzed in the "complex admittance plane"

Complex admittance plots are useful for determining an appropriate equivalent circuit for a system and for estimating the values of the circuit parameters. The complex impedance $Z(\omega)$ at an applied angular frequency ω can be expressed as:

$$Z(\omega) = Z_R(\omega) + j Z_I(\omega) \qquad (3.1)$$

or

$$Z(\omega) = |Z| e^{j\theta}$$

where the magnitude of the complex impedance $Z = \sqrt{Z_R^2 + Z^2}$, phase angle $\theta = \tan^{-1}(Z_I / Z_R)$ and Z_R is the real part and Z_I the imaginary part of the impedance. If one plot the imaginary part of the impedance $|Z_I|$ Vs $|Z_R|$ the real part, the resulting locus shows distinctive features for certain combinations of circuit elements. The method is best illustrated by specific examples of such plots shown in

Case (I) : Purely resistive circuit : If the circuit element or the sample under test is purely resistive then the complex impedance Z is given by,

$$Z(\omega) = R + j(0) \qquad (3.2)$$

Thus $\quad Z_R = R$ and $\qquad\qquad\qquad\qquad\qquad$ (3.3)

$\qquad Z_I = 0$ $\qquad\qquad\qquad\qquad\qquad\qquad\qquad$ (3.4)

or the complex admittance $Y(\omega)$ is given by

$$Y(\omega) = \frac{1}{2(\omega)} = \frac{1}{R + j(0)} = (-\frac{1}{R}) + j(0)$$

i.e. $Y_R = 1/R$ and $\qquad\qquad\qquad\qquad\qquad$ (3.5)

$\qquad Y_I = 0$ $\qquad\qquad\qquad\qquad\qquad\qquad\qquad$ (3.6)

CASE I

(i)

(ii)

CASE II

(iii)

(iv)
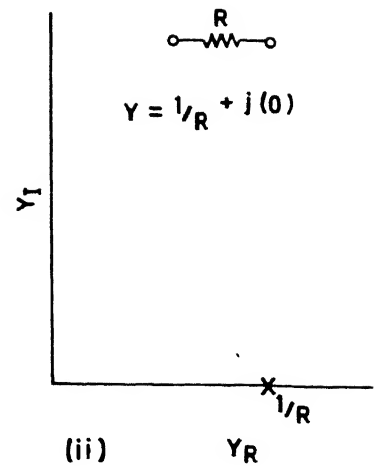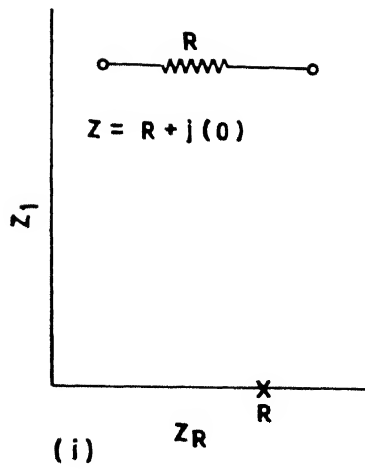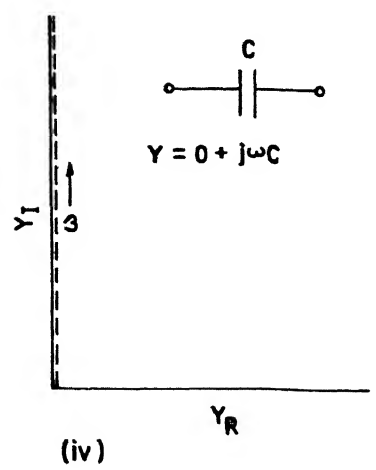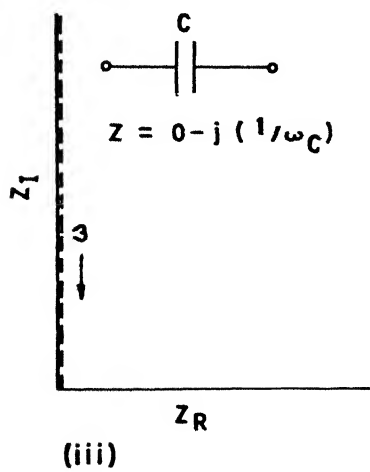
FIG. 3·1 (a) COMPLEX IMPEDANCE PLOTS

Thus for the case of pure resistance, the imaginary part of complex impedance/admittance is zero and the real part is constant at all frequencies, leading to a single point on the complex plane (see Fig. 3.1 (a) (i))

Case II : Purely capacitive Element:

In this case the complex impedance is given by

$$Z(\omega) = 0 - j \left(\frac{1}{\omega C} \right)$$

i.e., $Z_R = 0$ (3.7)

$$Z_I = \left(\frac{1}{\omega C} \right) \quad\quad\quad\quad\quad\quad (3.8)$$

or the admittance $Y(\omega)$ is given by

$$Y(\omega) = \frac{1}{Z(\omega)} = 0 + j(\omega C)$$

i.e., $Y_R = 0$ (3.9)

$$Y_I = \omega C \quad\quad\quad\quad\quad\quad (3.10)$$

Thus in this case the real part is zero and the imaginary part is linearly dependent on ω. The characteristic plot for this type of element is a straight line, coinciding with the imaginary axis (see Fig. 3.1 (a), (iii,iv). Note the difference between Fig. 3.1 (a) (iii) and 3.1 (a) (iv) as to the direction of ω.

Case III : Resistance and Capacitance in Series :

The complex impedance is given by

$$Z(\omega) = R + j(-1/\omega C)$$

so that $Z_R = R$ (3.11)

$$Z_I = -1/\omega C \quad\quad\quad\quad\quad (3.12)$$

or the admittance $Y(\omega)$ is given by

CASE III

R   C
$$Z = R - j\left(\frac{1}{\omega C}\right)$$

$$Z = \frac{R}{R^2 + 1/\omega^2 c^2} + j \frac{1/\omega c}{R^2 + 1/\omega^2 c^2}$$

CASE IV

$$Z = \frac{C \quad R}{R^2 \omega^2 c^2 + 1} - \frac{R^2}{R^2 \omega c + 1/\omega c}$$

$$Z = 1/R + j\omega C$$
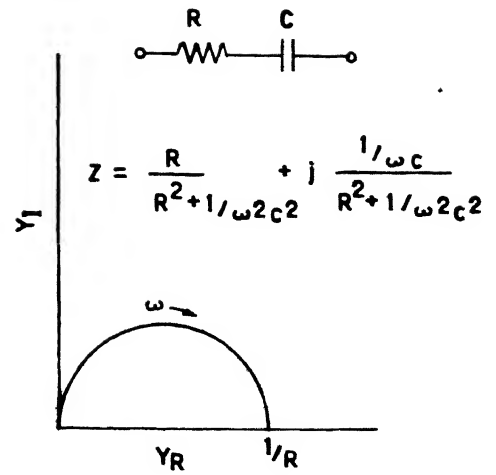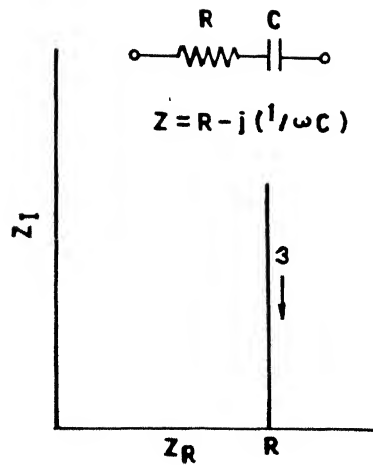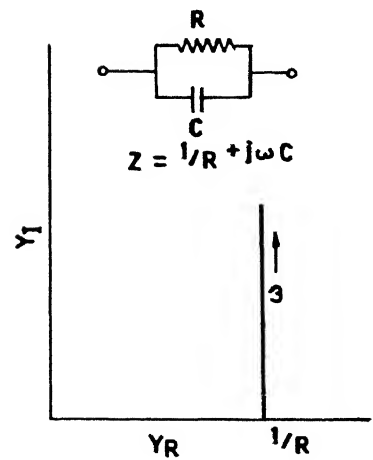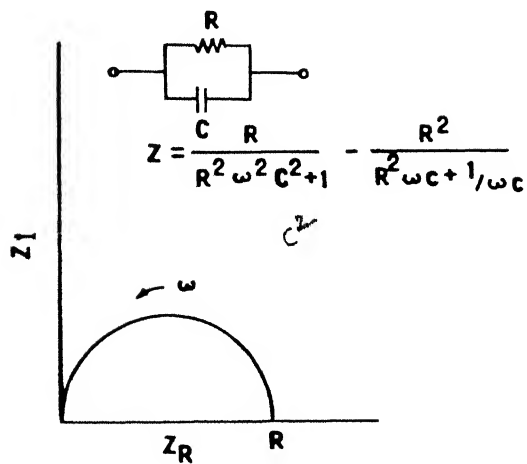
FIG. 3·1(b) COMPLEX IMPEDANCE PLOTS

$$Y(\omega) = \frac{1}{Z(\omega)} = \frac{1}{R + \frac{1}{j\omega C}} = \frac{R}{(R^2 + 1/\omega^2 C^2)} + j\frac{1/\omega C}{R^2 + 1/\omega^2 C^2}$$

i.e.
$$Y_R = \frac{R}{R^2 + 1/\omega^2 C^2} \qquad\qquad (3.13)$$

$$Y_I = \frac{1/\omega C}{R^2 + 1/\omega^2 C^2} \qquad\qquad (3.14)$$

The locus of the points ($Z_R = R$, $Z_I = -1/\omega C$) given by Eqs. 3.11 is a straight line parallel to Z_I axis and passing through the point (R,0), see Fig. 3.1 (b). The intercept with the real axis gives the magnitude of resistance R.

On the other hand, the locus of the points (Y_R, Y_I) defined by Eqs. 3.13 and 3.14 can be shown to be a circle of radius R/2 and centered at (R/2, 0). To show this we eliminate ω by squaring Eqs. 3.13 and 3.14 and then adding up,

$$Y_R^2 + Y_I^2 = \frac{R^2}{(R^2 + \frac{1}{\omega^2 C^2})^2} + \frac{(1/\omega C)^2}{(R^2 + \frac{1}{\omega^2 C^2})^2} =$$

$$\frac{1}{R^2 + (1/\omega C)^2}$$

using Eq. (3.13), the above equation reduces to

$$Y_R^2 + Y_I^2 = \frac{Y_R}{R}$$

OR
$$(Y_R - \frac{1}{2R})^2 + Y_I^2 = (\frac{1}{2R})^2 \qquad\qquad (3.15)$$

which has the form of $(x-a)^2 + y^2 = a^2$ which is an equation of a circle of radius 'a' having its center at (a,o). By analogy Eq. 3.15 represents a circle of radius $\frac{1}{2R}$ having its center at $(\frac{1}{2R}, 0)$ R being the resistance of the circuit. Thus the inverse of the diameter of the circle yields the resistance R of the sample/circuit element, see Fig. 3.1 (b).

Case IV Resistance and Capacitance in Parallel:

In this case the impedance $Z(\omega)$ is given by

$$Z(\omega) = \frac{R(1/j\omega C)}{R + 1/j\omega C} = \frac{R}{1 + \omega^2 C^2 R^2} + j \frac{-R^2 \omega C}{1 + \omega^2 C^2 R^2}$$

so that

$$Z_R = \frac{R}{1 + \omega^2 C^2 R^2} \qquad (3.16)$$

$$Z_I = \frac{-R^2 \omega C}{1 + \omega^2 C^2 R^2} \qquad (3.17)$$

on the other hand the admittance $Y(\omega)$ is given by

$$Y(\omega) = \frac{1}{Z(\omega)} = \frac{R + 1/j\omega C}{R/j\omega C} = \frac{1}{R} + j (\omega C)$$

so that

$$YR = \frac{1}{R} \qquad (3.18)$$

$$Y_I = \omega C \qquad (3.19)$$

The locus of the points defined by Eqs. 3.16 and 3.17 is attained by eliminating ω. As in the preceding case, we square Eqs. 3.16 and 3.17 and then add up to obtain

$$\theta = \tan^{-1} \left({}^{Z}I/_{Z_R} \right), \text{ so that}$$

$$Z(\omega) = Z \, e^{j\theta} = Z \, \cos\theta + j \, Z \, \sin\theta$$

$$Z_R = |Z| \cos\theta$$

$$Z_I = |Z| \sin\theta$$

Thus in actual practice Z and θ were measured and thereby the real part of the impedance $Z \cos\theta$ and the imaginary part Z $Z \sin\theta$ were calculated at a fixed temperature and for various frequencies. The plot of $|Z| \cos\theta$ Vs. $|Z| \sin\theta$ were usually circular suggesting that the LiBr-Al$_2$O$_3$ samples can be modelled by a parallel combination of R and C (case IV of the previous section), and that the diameter of the circle yields the resistive part R of the sample.

It must be emphasized that measurement of conductivity following the complex impedance analysis demands much greater effort and patience. For example, to obtain the σ at just one temperature, $|Z|$ and θ have to be measured at several different frequencies, the $|Z \cos\theta|$ Vs. $|Z \sin\theta|$ plot has to be made and only then the value of resistance can be extracted from the semicircular plot. To illustrate the total effort involved, we quote the data for only one composition, LiBr+ 20 mole %. Al$_2$O$_3$, and only at one temperature (306.5°C) in Table 3.1 which gives the measured parameters Z and θ at 20 different frequencies. The calculated parameters $|Z \cos\theta|$ and $|Z \sin\theta|$ are also listed in Table 3.1.

TABLE 3.1

Composition	: LiBr + 20 m/o Al_2O_3
Particle size of Al_2O_3	: 0.05 μ
wt. of alumina used	: 0.4506g
wt. of LiBr used	: 1.5592g
Pelletizing pressure	: 4 ton/cm^2
Dimensions of pellet	: length (l) = 0.406 cm, Area (A) = 0.95cm^2
Temperature	: 306.5 °C

Impedance data :

Frequency	Z (KΩ)	θ (deg.)	|Z sin θ|	|Z cos θ|
10 Hz	7.022	-9.47	1.1550	6.9263
20 Hz	6.655	-7.55	0.8744	6.5973
30 Hz	6.496	-6.59	0.7455	6.4530
0 Hz	6.317	-5.48	0.6032	6.2881
100 Hz	6.138	-4.34	0.4644	6.1203
200 Hz	5.997	-3.46	0.3619	5.9860
300 Hz	5.936	-3.08	0.3189	5.927
500 Hz	5.867	-2.71	0.2773	5.860
1KHz	5.787	-2.43	0.2453	5.7817
3KHz	5.684	-2.68	0.2657	5.6777
5KHz	5.643	-3.25	0.3199	5.6339
10KHz	5.582	-4.85	0.4719	5.5620
30KHz	5.394	-11.15	0.0430	5.2921
50KHz	5.188	-16.98	1.5150	4.9618
100KHz	4.612	-29.24	2.2528	4.0243
200KHz	3.545	-45.59	2.4673	2.2807
300KHz	2.784	-55.21	2.2863	1.5884
500KHz	1.901	-65.43	1.7288	0.7904
1000KHz	0.9140	-8182	0.9047	0.1300
1500KHz	0.6204	-88.01	0.6200	0.0215

Fig. 3.2 shows the plot of Z Cosθ vs Z Sinθ for LiBr+ 20 mole% Al_2O_3 sample at 306.5°C (corresponding to the the data shown in Table 3.1) as well as at four other temperatures whose complex impedance data (Z,θ) are not included in this thesis. It is noted in Fig. 3.2 that Z Sin θ vs. Z Cos θ plots are nearly semicircular. the radius of the semicircle at 306°C is $\frac{R}{2}$ =2.907 KΩ which yields, according to Eq. 3.20, a value of R = 5.814 kΩ and the corresponding conductivity of 5.79 x 10^{-5} Ohm^{-1} Cm^{-1}. In this way, the conductivity is obtained at one temperature. In order to study the temperature dependence of conductivity of a particular composition, the complex impedance data and plots such as those shown in Fig. 3.2-r.4. Table 3.1 and Fig. 3.12 will have to be taken at many (15-20) different temperatures. This would then complete the electrical conductivity study for one particular composition. In this work eight different compositions have been studied, as discussed in the next section.

Figs. 3.3 and 3.4 show the complex impedance plots for LiBr+ 10mole% Al_2O_3 and LiBr+15mole% Al_2O_3 at some selected temperature just as fig. 3.2 shows for LiBr + 20 mole % Al_2O_3. However the impedance data tables for 10 and 15 mole % Al_2O_3 arenot included here, nor the impedance plots for several other compositions at different temperatures are shown in this chapter.

The complex impedance plots for three compositions, viz., LiBr + 10 mole % Al_2O_3, LiBr + 15 mole % Al_2O_3, and LiBr + 20 mole % Al_2O_3 shown respectively in Figs. 3.3, 3.4 and 3.2 are included in this chapter to make a point, namely, that the complex
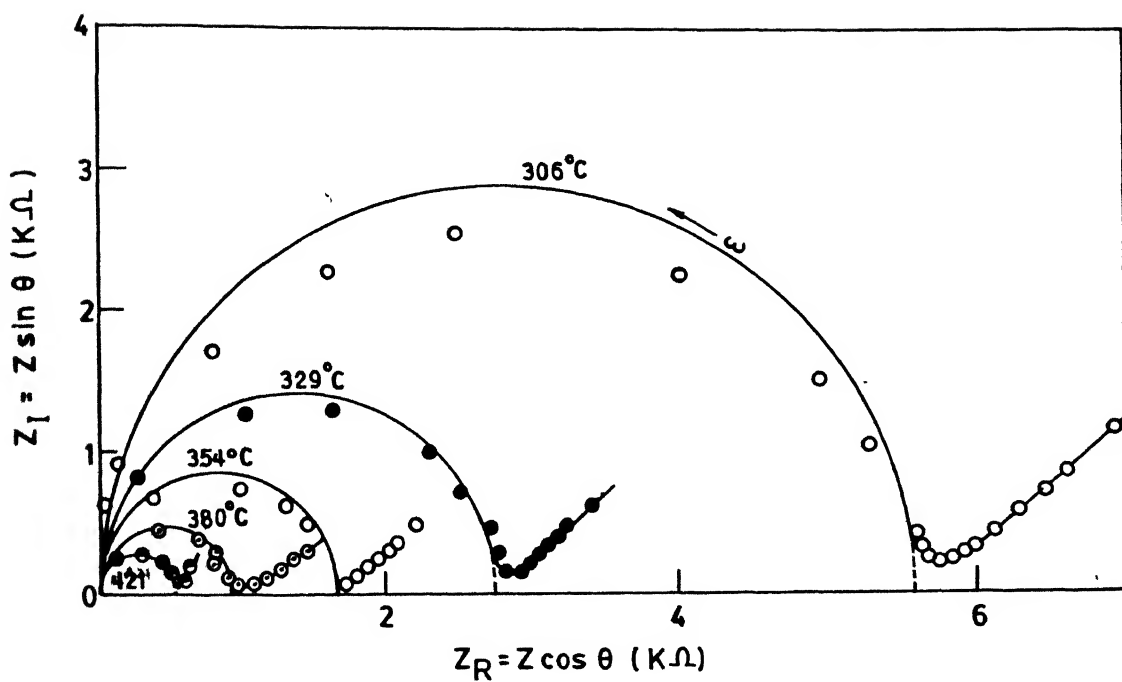
FIG. 3·2   COMPLEX IMPEDANCE PLOT FOR LiBr (20·m/o, Al₂O₃)

temperatures this can also be explained by the above relationship Eq. . 3.22 . As the temperature increases, the space change layer λ decreases and hence σ decreases. Also, as the temperature increases, thermally created lattice defects increase, and those defects introduced by charged surfaces of the dispersed particles play a smaller role in ionic transport. For a given temperature, the conductivity attains a maximum value at a critical mole fraction of added second phase as shown in Fig. 3.7. The decrease in conductivity for additions of more second phase is due to the fact that the volume occupied by the insulator particles becomes a large fraction of the total. Moreover, as the dispersed particles approach one another, there should be an optimum distance between the particles for maximum enhancement. In addition, the wetting of Al_2O_3 at high concentrations of Al_2O_3 may be less. All these have however not been proved quantitatively.

3.3 Variation of Conductivity with Temperature:

One of the characteristic features of the ionic conductivity of a solid salt is its variation with temperature. Fig. 3.9 shows a typical curve.

Two facts stand out plainly. The first is the existence of two main regions in the conductivity curve, the second is that in both these regions the logarithm of the conductivity is roughly a linear function of T^{-1}. The high temperature section of the curve, above the transition region or " knee", in general is an intrinsic property of the substance, and measurements in this region are quite reproducible. On the other hand, the low temperature
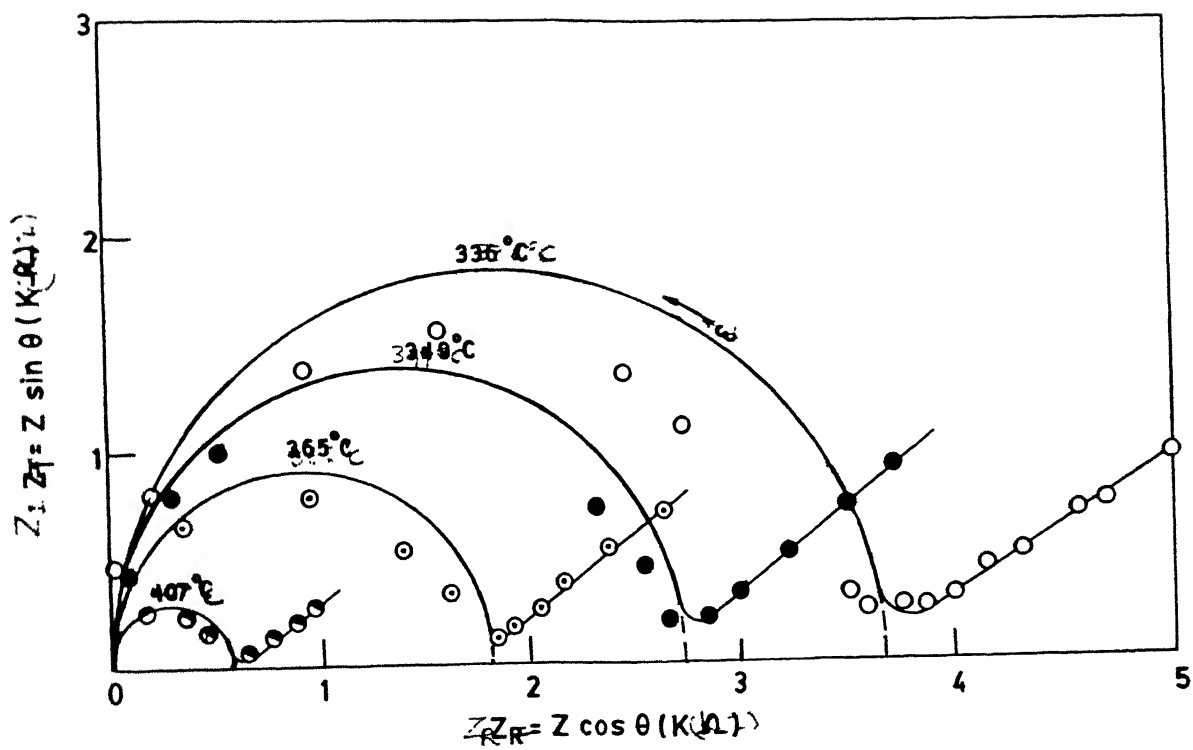
FIG. 3·4   COMPLEX IMPEDANCE ANALYSIS LiBr (15 m/o, Al_2O_3)

impedance plots are, by and large, circular suggesting that the
parallel combination of R and C model (case IV, Section 3.1)
is appropriate for LiBr-Al$_2$O$_3$ system. However, it should be pointed
out that in almost all the plots (Figs. 3.2 to 3.4) the curves
deviate from the circular behavior at lower frequencies. In
fact, the low frequency impedance plot ($|Z|$ Sin θ vs. $|Z|$ Cos θ) is
more or less linear.

In order to describe the frequency dispersion analysis, it
is useful to start from the well known Debye circuit, which is an
idealized equivalent circuit that often is used as a first approxi-
mation in the analysis of the frequency dependence of the admittance/
impedance of the solid-blocking electrode combinations. This
model Fig. 3.5 consists of an electrolyte-electrode interface
capacitance C_{int}, due to the ionically blocking electrodes, a bulk
ionic resistance R_i, and the geometric capacitance C_g which is
due to the simple parallel plate capacitance of the two electrodes,
with the sample as a dielectric medium between them. If the solid
is a reasonably good ionic conductor and the electrolyte- electrode
contact is good, the interface capacitance, C_{int}, is typically orders
of magnitude larger than the geometrical capacitance. This then
results in a clear separation of the frequency dispersion into a
low frequency interface-related part (the vertical straight line)
in which the behavior is dominated by the parallel arrangement of
R_i and C_g. The opposite holds for the complex admittance plot
(3.5c) where the semicircle represents the low frequency part, and
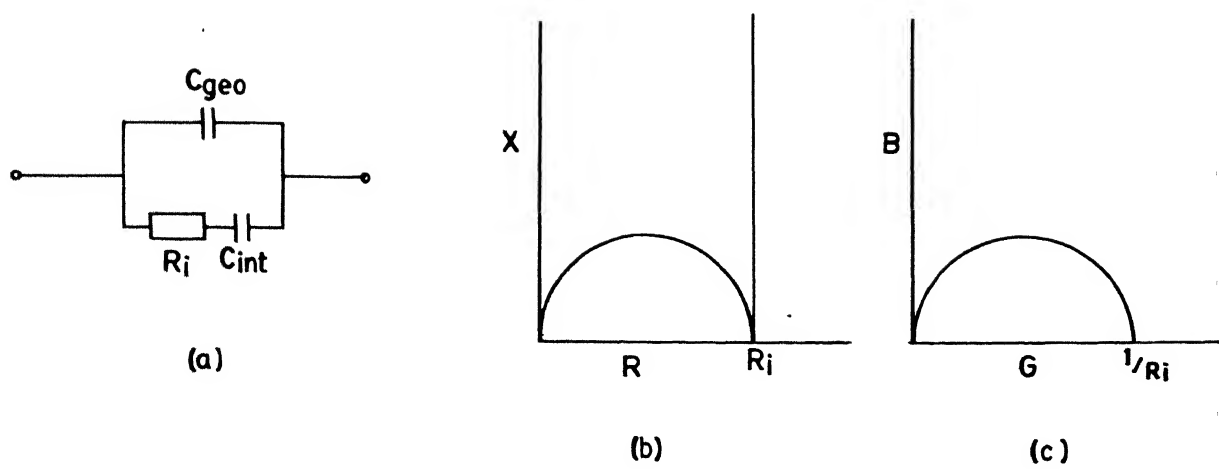the tail the high frequency region.

(a)

(b)

(c)

FIG. 3.5   AN IDEAL CIRCUIT FOR THE SOLID ELECTROLYTE / ELECTRODE SYST[

The real behaviour of the LiBr-Al$_2$O$_3$ system shown in Figs. 3.2 an 3.4 for various compositions show a low frequency tail which is not exactly similar to the proposed Debye circuit. This region may be considered to be consisting of a bulk (ionic) resistance R$_i$, an interface capacitance C$_{int}$ and a Warburg-like complex element, apparently due to diffusion processes near the electrolyte- electrode interface as reported for the Li$_3$N (Boukamp, 1978). The impedance of this complex element is of the form $Z(\omega) = A\omega^{-\alpha} - jB\omega^{-\alpha}$ where

has values between 0 and 1, and it has been shown that $B/A = \tan\alpha\pi/2$. The sign of the curvature indicates that the interface capacitance, C$_{int}$, and the Warburg like element are in series, rather than in parallel. The equivalent circuit is shown in Fig. 3.6.

3.1.2 Comparision of onductivity at 1khz with that Obtained from CIA:

It is worthwhile to compare the conductivity obtained from the complex impedance analysis (CIA) with the conventional a.c. (1khz) conductivity. It is obvious from Table 3.2 that the two values are not very different from each other which may be fortuitou For many a systems the conductivity inferred from the CIA is less than/the a.c. conductivity at 1khz . This is particularly true for polycrystalline solids, as these samples have a lot more grain boundaries and therefore the sample capacitance is large (reactance 1/Cω is small)

3.2 VARIATION OF CONDUCTIVITY WITH COMPOSITION :

The conductivity of LiBr was found to depend strongly on the concentration of dispersed phase γ-Al$_2$O$_3$. The conductivity
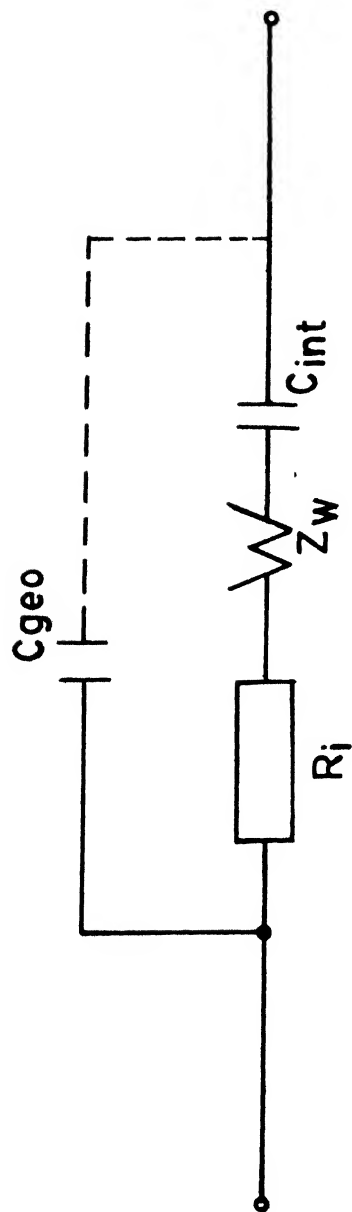
FIG.3.6 EQUIVALENT CIRCUIT

TABLE 3.2

Comparison of conventional ac (1KHz) conductivity with that obtained
by the complex impedance analysis (CIA) for LiBr- 20 m/o Al_2O_3

$T^\circ C$	ac (1KHz) conductivity $(-\Omega^{-1} cm^{-1})$	Conductivity for CIA $(\Omega^{-1} cm^{-1})$
87	1.08×10^{-5}	1.08×10^{-5}
105	2.11×10^{-5}	2.13×10^{-5}
125	4.66×10^{-5}	4.19×10^{-5}
145	1.39×10^{-4}	1.17×10^{-4}
165	1.53×10^{-4}	1.50×10^{-4}
185	2.47×10^{-4}	2.40×10^{-4}
205	4.28×10^{-4}	3.97×10^{-4}
225	7.72×10^{-4}	7.15×10^{-4}
250	1.12×10^{-3}	1.09×10^{-3}
205	1.35×10^{-3}	1.32×10^{-3}

Vs. composition plot (Fig. 3.7) exhibits a rather flat maximum at 10 mole % Al_2O_3 (0.05 μm). As the concentration of Al_2O_3 increases further the conductivity shows a decreasing tendency over the entire composition range studied. However, the conductivity corresponding to 15 mole % Al_2O_3 shows a marked decrease in conductivity which is rather supprising. The maximum conductivity obtained was $6.9 \times 10^{-6} \Omega^{-1}$ c at 84°C for 10 mole % Al_2O_3 sample. The maxima at 10 mole % Al_2O_3 is not very sharp probably due to the presence of moisture in the samples. Both LiBr and $\gamma - Al_2O_3$ used were undried. While this work was in progress we came to know about a recent paper on LiBr-Al_2O_3 by Khandkar and Wagner (1986) who also report an enhancement in σ by the dispersion of Al_2O_3 particles. However, the magnitude of enhancement in σ and the composition corresponding to the maxima in the conductivity vs. composition plot are different in the two studies. We found a maximum ehancement of nearly 4 orders of magnitude vs 1 order reported by Khandkar and Wagner (1986). It is possible that the presence of moisture in our case leads to larger enhancement We used both LiBr and Al_2O_3 without drying.

It has also been observed that the conductivity is an inverse function of the particle size of the dispersoid, i.e. the enhancement is longer if the dispersed particles are of smaller size. Table 3.3 gives the values of conductivities for two different particles i.e. 0.5μm and 30 μm at three different temperatures for 10 mole% Al_2O_3. This is in agreement with the theoretical model put forward by Jow and Wagner (1979) for the CuCl (Al_2O_3) system. According to their model, the enhancement in conductivity due to the presence of the second dispersed phase is given by,
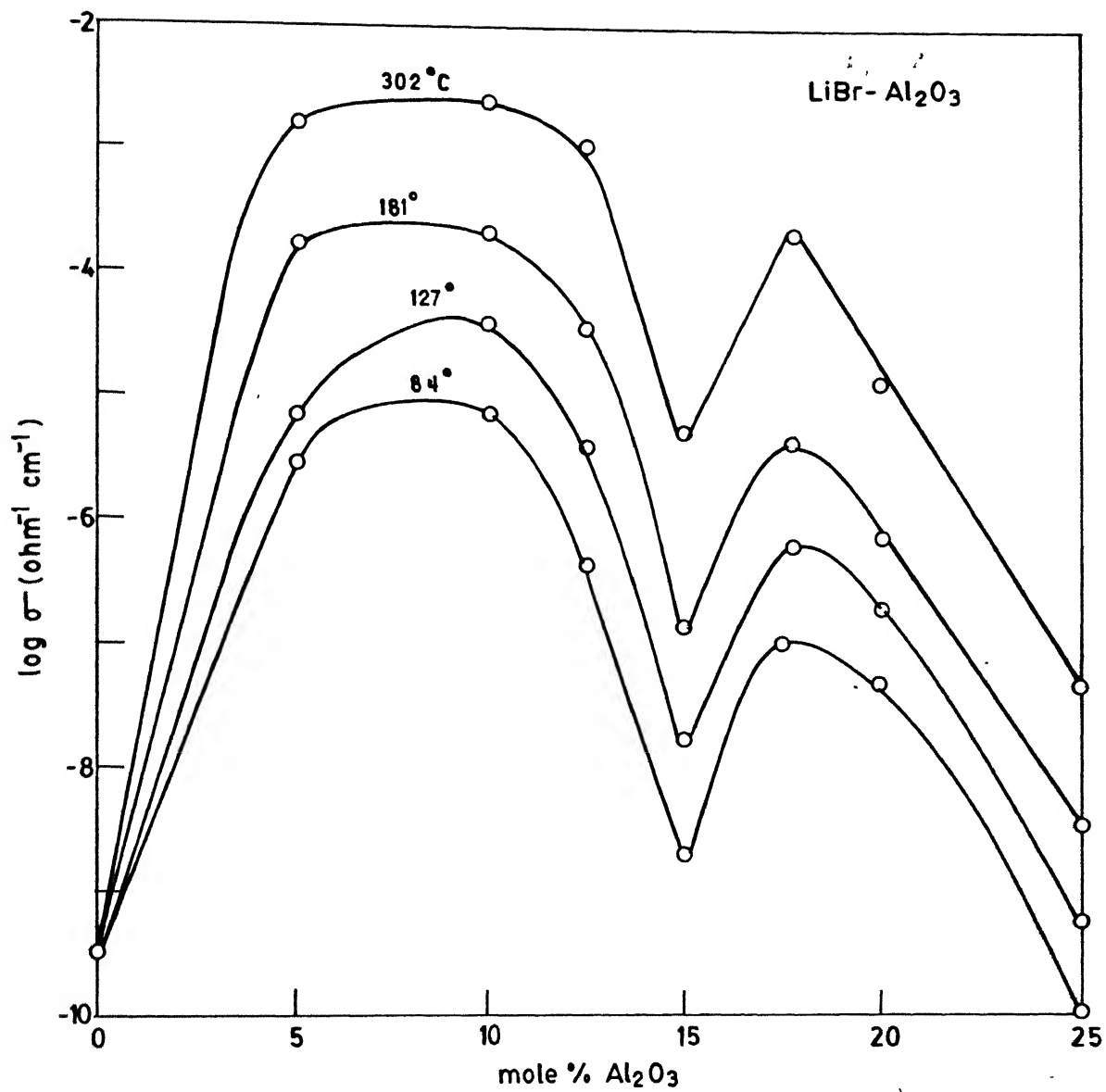
FIG. 3.7   VARIATION OF CONDUCTIVITY WITH COMPOSITION

TABLE 3.3

Variation of Conductivity with Particle Size

Mole fraction of Al_2O_3	Temp. (°C)	r (μm)	σ $(\Omega^{-1}cm^{-1})$
10 m/o	200	0.05	3.40×10^{-4}
10 m/o	205	30	7.86×10^{-6}
10 m/o	232	0.05	5.78×10^{-4}
10 m/o	236	30	1.56×10^{-5}
10 m/o	258	0.05	9.02×10^{-4}
10 m/o	259	30	3.45×10^{-5}
10 m/o	291.5	0.05	2.52×10^{-3}
10 m/o	297	30	4.80×10^{-5}

$$\Delta \sigma = 3 \sum_i e\mu_i \langle \Delta n_i \rangle \frac{\left(\dfrac{r_1}{r_2} \right)^3}{\left[1 - \left(\dfrac{r_1}{r_2} \right)^3 \right]} \qquad (3.21)$$

where

μ_i =   mobility of defects

$\langle \Delta n_i \rangle$ =   average excess charge density

r_1 =   radius of the alumina particle

r_2 =   half the average distance between two alumina particles

In the case where r_2 r_1 , $(r_1/r_2)^3$ can be approximated to V_v (the volume fraction of the dispersoid) the relation Eq. 3.12 reduces

to $\Delta \sigma = 3 \sum_i e\mu_i \langle \Delta n_i \rangle \; \lambda \left(\dfrac{1}{r_1} \right) \left(\dfrac{V_v}{1-V_v} \right) \qquad r_2 > r_1 \qquad (3.22)$

Since μ_i, $\langle \Delta n_i \rangle$ and λ are all functions of temperature, at

a definite temperature, the excess conductivity $\Delta \sigma$

$$\Delta \sigma \propto \left(\frac{1}{r_1} \right) \left(\frac{V_v}{1-V_v} \right)$$

Thus the plot of total conductivity Vs. $(1/r_1) \left(\dfrac{V_V}{1-V_v} \right)$ should

be linear. Fig. 3.8 shows this plot for our sample. A linearity

is observed at lower concentration of Al_2O_3 (5 m/o, 10 m/o)

i.e. where the relation r_2 r_1 still holds. At larger concentrations

since r_2 is not much larger than r_1 there is a considerable

deviation from a straight line. It has also been observed in

the log σ vs. 1/T plots Fig. 3.10 that the conductivity

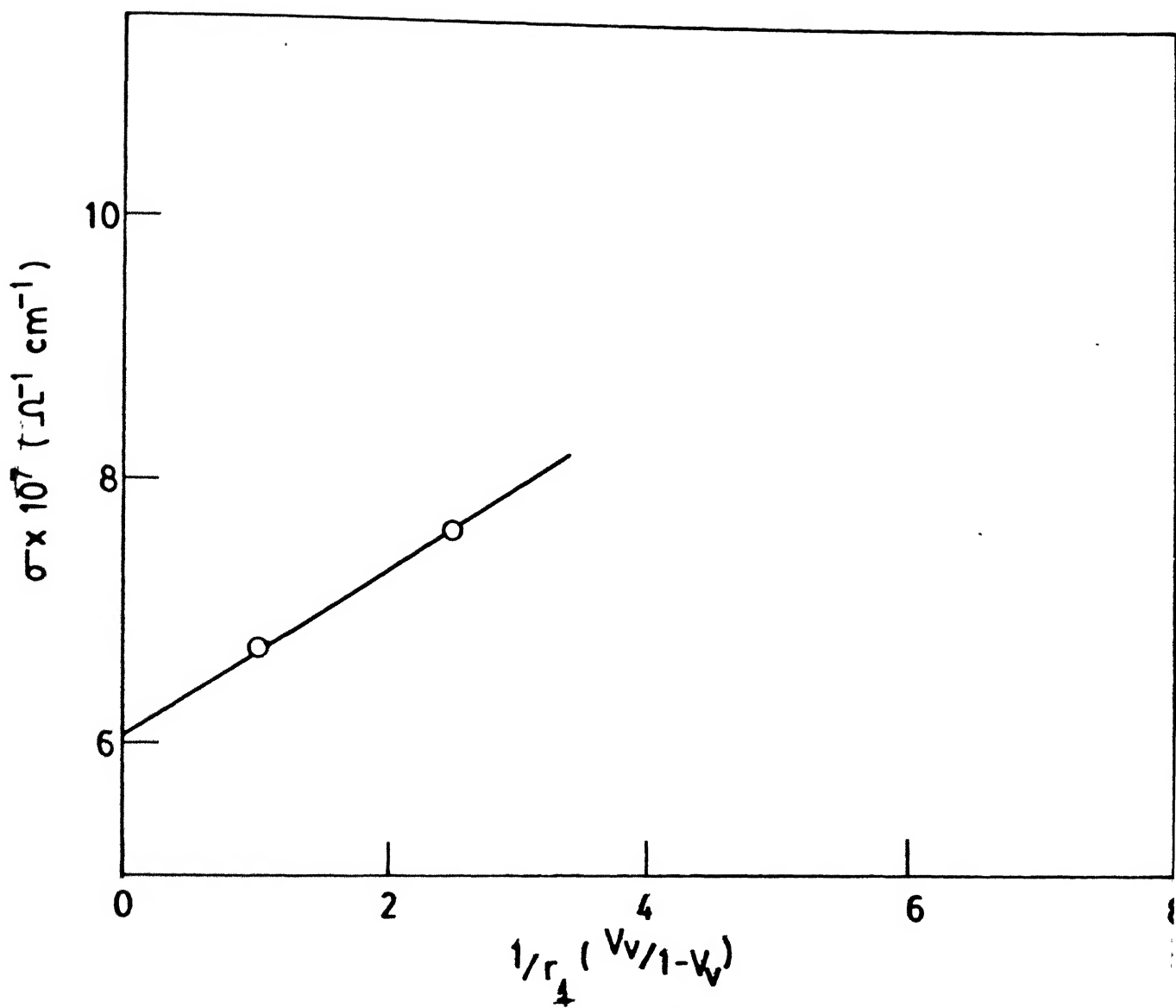enhancement is greater at low temperatures and lesser at high

FIG. 3·8   CONDUCTIVITY Vs. $[^1/r_1 \cdot {}^{V_V}/_{1-V_V}]$ AT 84° C

temperatures this can also be explained by the above relationship
Eq.. 3.22 . As the temperature increases, the space change layer λ
decreases and hence σ decreases. Also, as the temperature
increases, thermally created lattice defects increase, and those
defects introduced by charged surfaces of the dispersed particles
play a smaller role in ionic transport. For a given temperature,
the conductiwity attains a maximum value at a critical mole fraction
of added second phase as shown in Fig. 3.7. The decrease in
conductivity for additions of more second phase is due to the fact
that the volume occupied by the insulator particles becomes a large
fraction of the total. Moreover, as the dispersed particles
approach one another, there should be an optimum distance between
the particles for maximum enhancement. In addition, the wetting
of Al_2O_3 at high concentrations of Al_2O_3 may be less. All these
have however not been proved quantitatively.

3.3 Variation of Conductivity with Temperature:

One of the characteristic features of the ionic conductivity
of a solid salt is its variation with temperature. Fig. 3.9 shows
a typical curve.

Two facts stand out plainly. The first is the existence of
two main regions in the conductivity curve, the second is that in
both these regions the logarithm of the conductivity is roughly
a linear function of T^{-1}. The high temperature section of the
curve, above the transition region or " knee", in general is an
intrinsic property of the substance, and measurements in this
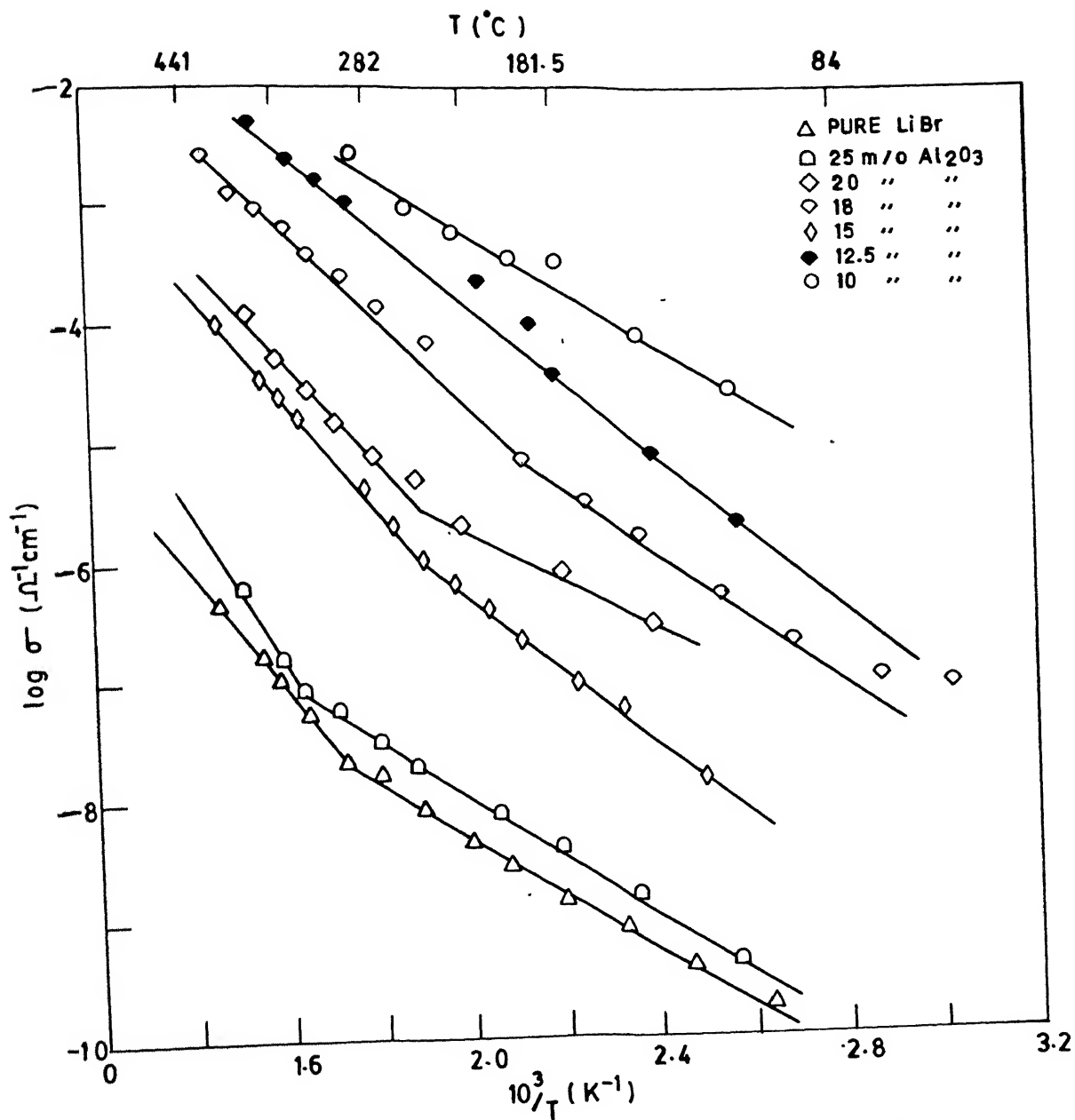region are quite reproducible.On the other hand, the low temperature

FIG. 3·9   VARIATION OF CONDUCTIVITY WITH TEMPERATURE

conductivity not only displays a smaller slope but depends in magnitude on the particular specimen employed and to some extent on its thermal history. The complete conductivity curve is therefore roughly a superposition of two curves,

$$(1) \quad \sigma = \sigma_1 \exp(-Ea_1/kT) \quad \text{(low temperature part or extrinsic region)}$$

$$(2) \quad \sigma = \sigma_1 \exp(-Ea_2/kT) \quad \text{(high temperature part or intrinsic region)}$$

The energy Ea_1 is less than Ea_2, and $\sigma_1 < \sigma_2$. The slope of the log σ vs $1/T$ plot in the low temperature (extrinsic) region yields Ea_1 which is the activation energy of migration of the more mobile species. In LiBr-Al$_2$O$_3$ system, E_{a1} must be interpreted as the migration energy of Li$^+$-vacancies. The slope of the logσ vs. $1/T$ plot in the intrinsic region yields Ea_2 which is the sum of half of formation energy and migration energy i.e.,

$$Ea_2 = \frac{H_s}{2} + h_m \quad \text{(intrinsic)}$$

$$Ea_1 = h_m \quad \text{(extrinsic)}$$

Thus the two slopes in the logσ vs $1/T$ plots can be used to determine the migration and formation energy of the defects.

Fig. 3.9 shows the variation of logσ vs. $1/T$ for a number of LiBr-Al$_2$O$_3$ composites. The conductivity of LiBr + 10 mole % A Al$_2$O$_3$ is highest at all temperatures. The activation energies

and preexponential factors calculated from the linear plots are summarized in Table 3.4. The conductivity and activation energies for pure LiBr are in agreement with the literature data on polycrystalline material (Khandkar and Wagner, 1986). From Fig. 3.9 it can be noticed that as the concentration of Al_2O_3 increases the conductivity increases consistently upto 10 m/o Al_2O_3. However, the extrinsic to intrinsic transition temperature, referred to as "Knee" temperature is absent for 10 m/o at 12.5 m/o Al_2O_3 compositions. It is possible that knee has shifted to higher temperatures for these compositions, and therefore not visible in the plot. This is in line with the fact that effect of doping or producing excess defects is to enlarge the range of extrinsic conduction.

If we consider the effect of dispersion of Al_2O_3 is to generate excess of mobile lattice defects i.e. the dispersoids act as a kind of macro-dopants, then the increase in the conductivity, enlargement of the range of extrinsic region, etc. as observed are self consistent, the activation energy of 0.43 eV for LiBr + 10 % Al_2O_3 is very close to that (0.46 eV) of pure LiBr, suggesting that the conduction in 10% Al_2O_3 sample is not due to thermally activated defects but due to defects produced by Al_2O_3 particles around its surface.

3.4 SEM STUDIES :

The SEM studies were undertaken to determine the micro-structure and the distribution pattern of the dispersed Al_2O_3

TABLE 3.5

Results on Some Dispersed Solid Electrolyte Systems

Material	Dispersoid and its size (μm)	m/o of dispersoid for maximum enhencement	Temperature °C	Maximum enhancement in σ by a factor of	Reference
LiI	I_2O_3 (unknown)	40	25	100	Liang (1973)
LiI	Al_2O_3 (unknown)	50	25	50	von Alpen and Bell (1979)
$LiI.H_2O$	Al_2O_3 (0.3)	24	25	100	Pack, et.al. (1980)
CuCl	Al_2O_3 (0.06)	10	60	50	Chang et al. (1979)
AgI_2	Al_2O_3	30	203	100	S. Pack (1979)
AgI	dried Al_2O_3 (0.06)	30	25	50	Shahi et al. (1981)
AgI	SiO_2 (0.007)	1	25	45	Shahi et al (1981)
LiBr	Al_2O_3 (0.06)	20	127	50	Khandkar et al (1986)
LiBr	Al_2O_3 (0.05)	10	84	10^4	This work

TABLE 3.4

Ionic Conductivity, Activation Energy, and Pre-exponential Factor for LiBr-Al$_2$O$_3$ Composites

Material	E_a (eV)	Temperature range (°C)	σ_o (Ohm^{-1} cm^{-1})	σ at T°C (Ohm^{-1} cm^{-1})
Pure LiBr	0.94 0.46	305–411 38–305	3.56 x 10^{-5} 1.26 x 10^{-5}	3.11 x 10^{-7} at 100°C 2.58 x 10^{-9} at 200°C
LiBr + 10 m/o Al$_2$O$_3$	0.45	127–360	20.8	3.55 x 10^{-4} at 200°C
LiBr + 12.5 m/o Al$_2$O$_3$	0.72	89–368	3.16 x 10^{3}	6.46 x 10^{-5} at 200°C
LiBr + 15 m/o Al$_2$O$_3$	0.90 0.57	253–407 156–253	4.92 x 10^{3} 2.92	2.34 x 10^{-4} at 350°C 2.27 x 10^{-6} at 200°C
LiBr + 18 m/o Al$_2$O$_3$	0.61	58–419	2.95 x 10^{2}	1.12 x 10^{-5} at 200°C
LiBr + 20 m/o Al$_2$O$_3$	0.75 0.39	308–421 154–308	5.74x10^{2} 25.4	4.61 x 10^{-4} at 350°C 8.1 x 10^{-6} at 200°C
LiBr + 25 m/o Al$_2$O$_3$	1.32 0.45	336–389 27–336	5.98 x 10^{4} 4.06 x 10^{-3}	1.24 x 10^{-6} at 350°C 5.7 x 10^{-8} at 200°C

particles. The pellets which/earlier used for σ studies, were

were

produced and small portions of these were mounted on a circular

aluminium plate with quickfix. Silver paint was painted on the

edges of the particle plate was then kept in a vacuum jar and

The

evacuated to 10^{-5} mm Kg with slight heating to get rid of the mixture

on the surface of the sample. These were then coated with a

conducting layer of silver by vacuum deposition. Then the speci-

men were ready for SEM observations.

The various SEM micrographs are displayed in Figs. 3.10 -

3.12. It must be pointed out that the results not very instructive

since the specimen were highly hygroscopic leading to poor contrast.

Comparison of 3.10 and 3.11 show the difference in microstructure

of pure LiBr and that containing $-Al_2O_3$. The particle size

Al_2O_3 calculated from 3.11 is found to be 0.5 μm. This would

indicate that the Al_2O_3 particles get agglomerated in various stages

of sample processing. The another noteworthy point is that dis-

persion of the alumina particles was not very uniform. This was

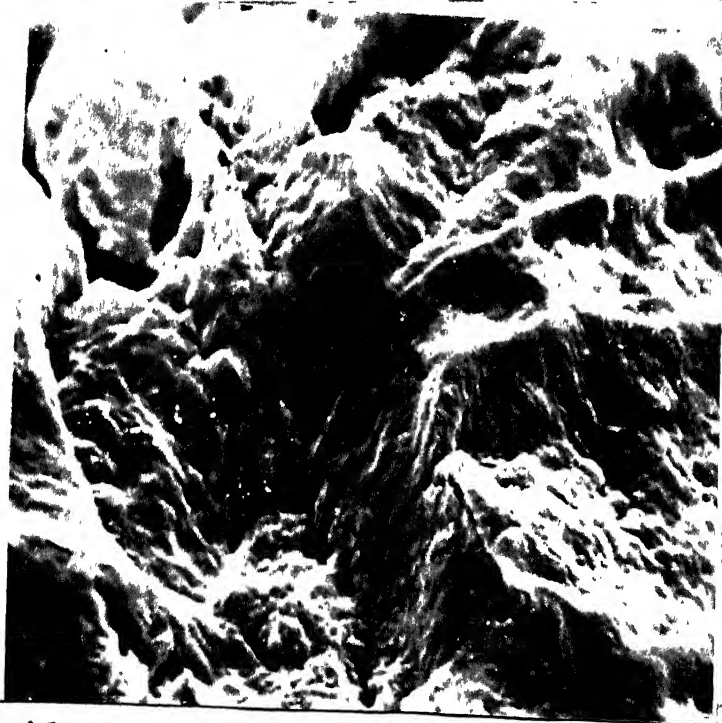concluded by scanning different areas of the same sample.
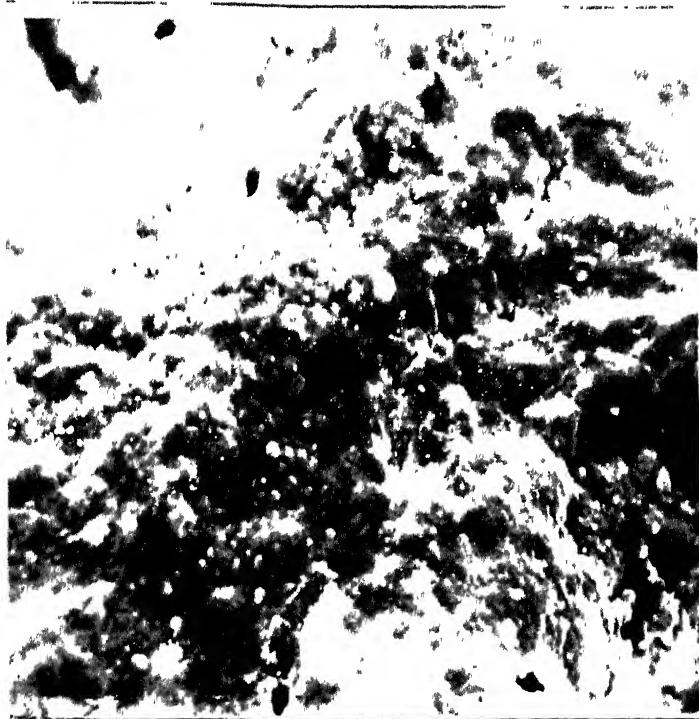
Fig. 3.10 Surface of pure LiBr (2100 x)

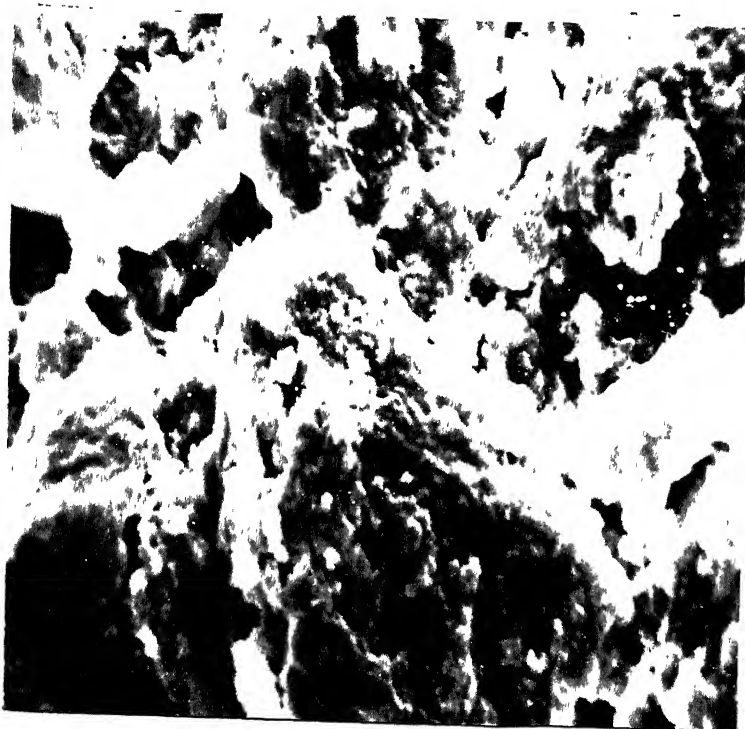Fig. 3.12   Surface of LiBr containing 20 m/o Al_2O_3 of 0.05 μm initial particle (2100x).

Fig. 3.11 Surface of LiBr containing 10 m/o Al_2O_3 of 0.05 μm initial particle size (2100x).

CONCLUSION :

The present study investigates the enhancement in conductivity due to dispersion of fine insulating particles. The system which has been examined is $LiBr-Al_2O_3$. It should be stressed at the outset that both LiBr and Al_2O_3 are very difficult materials to work with. Both of them are very hygroscopic affecting the reproducibility of the data.

Complex impedance analysis has been used extensively and satisfactorily. Most of our samples can be modelled by a parallel combination of resistance and capacitance.

Our studies confirm further that the dispersion of fine insulating particles indeed enhance the conductivity significantly, It has been found that LiBr containing 10 m/o Al_2O_3 of 0.05 μm size can increase the conductivity by as much as 4 orders of magnitu The best conductivity achieved is $10^{-5} Ohm^{-1} cm^{-1}$ at 84°C for LiBr + 10% Al_2O_3 while the σ of LiBr is $10^{-9} Ohm^{-1} cm^{-1}$ at the same temperature.

Our results suggest that the presence of water either in the host matrix or with the dispersoid tends to increase the σ further. The effect of the particle size of the dispersoids could not be studied in detail as we had only two different sizes of Al_2O_3 particles. The space-charge model of Jow and Wagner (1979) appears satisfactory for limited concentrations of dispersoids.

The dispersion of Al_2O_3 particles can be treated as a phenomenon of "macro-doping", in analogy with microscopic-doping of ionic solids by aliovalent ions, e.g. $AgI : Cd^{2+}$. In the latter case the dopant ion occupies the host-lattice and

produces excess of defects leading to higher conductivity etc. In the former, i.e. the dispersed phase solid electrolyte, the dispersoid does not form solid solubility, but creates extra surfaces around which are produced extra defects that increase the conductivity.

In view of the fact that the dispersed phase solid electrolytes are quite stable in battery environments, it would be worth pursuing these studies further.

REFERENCES :

1. Baurle, S.E. J. Phys. Chem. Solids $\underline{30}$, 2657-2670 (1970)

2. Biefeld, R.M. and R.T. Johnson Jr. J. Electrochem. Soc. $\underline{126}$, 1 (1979).

3. Boukamp, B.A. and Huggins, R.A. Mat. Res., Bull. $\underline{13}$, 23 (1978).

4. Chandra, S., Superionic Solids, Principles and Applications (North-Holland, 1981).

5. Crosbie, G., J. Solid State Chem. $\underline{25}$, 367 (1978).

6. Friauf., R.J., in Physics of Electrolytes Vol. 1 and 2 ed. J. Hladik, Academic Press, London (1972).

7. Geller, S., Solid Electrolytes (Springer-Verlag, 1977).

8. Huggins, R.A. Electrochemica Acta, $\underline{22}$, 773-781 (1977).

9. Jow, T. and J.B. Wagner Jr. J. Electrochem. Soc. $\underline{126}$, 163 (1979).

10. Khandkar, A. and J.B. Wagner Jr. Solid State Ionics $\underline{20}$, 257 (198

11. Kliever, K.L. and J.S. Koehler, Phys. Rev. A., $\underline{140}$, 1226 (1965).

12. Kliever, K.L. J. Phys. Chem. Solids. 27, 705, (1966).

13. Landauer, R. J. Appl. Phys. $\underline{23}$, 779 (1952).

14. Lehovec, K. J. Chem. Phys. $\underline{21}$, 1123 (1953).

15. Liang, C.C. J. Electrochem. Soc. $\underline{120}$, 1289 (1973).

16. Liang, C.C., A.V. Joshi and N.E. Hamilton J. Appl. Electrochem.

17. Lidiard, A.B. in Handbuch der Physik ed. S. Plugge, $\underline{20}$, p. 246 (Springer-Verlag) (1957).

18. Magistrics, A., A. Schiraldi and G. Chiodellic, Electro-chemica acta $\underline{22}$, 689-692 (1977).

19. Pack, S., B.B. Owens and J.B. Wagner, Jr. J. Electrochem. Soc. $\underline{127}$, 2177 (1980).

20. Raleigh, Lord, Phil. Mag. $\underline{34}$, 481 (1992).

21. Rice, M.J. and W.L. Roth, J. Solid State Chem. $\underline{4}$, 294-316 (1972).

22. Shahi, K., Phys. State. Solidi, $\underline{41}$, 11 (1977).

23. Shahi, K. and J.B. Wagner, Jr. Appl. Phys. Lett. 37, 757 (1980).

24. Shahi, K. and J.B. Wagner Jr. J. Electrochem. Soc. 128, 6 (1981).

25. Shahi, K. and J.B. Wagner, Phys. Rev. B. 23, 6417-6421 (1981)

26. Shahi, K. and J.B. Wagner, Solid State Ionics 3/4, 295-299 (1981).

27. Shahi, K. and J.B. Wagner, J. Solid State Chem. 42, 107-119 (1982).

28. Shahi, K. and J.B. Wagner, J. Phys. Chem. Solids 44 (2), 89-94 (1983).

29. Shahi, K. and J.B. Wagner, Solid State Ionics 12, 511-516 (1984

30. Stoneham, A.M., E. Wade and J.A. Kilner Mat. Res. Bull. 14, 661 (1979).

31. Wagner, C. J. Phys. Chem. Solids 33, 1051 (1972)

32. von Alpen, U and M.F. Bell in Fast Ion Transport In Solids, Electrodes and Electrolytes ed. P. Vashishth, J.N. Mundy G.K. Shenoy (North Holland).